Table 1. List of the 232 SNIa explosion models with yields from the literature tested with our method.

Model Name	Ref.	Basic Proprieties
Fi14_N1def	1	3D deflagration, $\rho_{c,9}$ = 2.9, 1 slightly off-centre ignition bubbles
Fi14_N3def	1	3D deflagration, $\rho_{c,9}$ = 2.9, 3 centred ignition bubbles
Fi14_N5def	1	3D deflagration, $\rho_{c,9}$ = 2.9, 5 centred ignition bubbles
Fi14_N10def	1	3D deflagration, $\rho_{c,9}$ = 2.9, 10 centred ignition bubbles
Fi14_N20def	1	3D deflagration, $\rho_{c,9}$ = 2.9, 20 centred ignition bubbles
Fi14_N40def	1	3D deflagration, $\rho_{c,9}$ = 2.9, 40 centred ignition bubbles
Fi14_N100Hdef	1	3D deflagration, $\rho_{c,9}$ = 5.5, 100 centred ignition bubbles
Fi14_N100def	1	3D deflagration, $\rho_{c,9}$ = 2.9, 100 centred ignition bubbles
Fi14_N100Ldef	1	3D deflagration, $\rho_{c,9}$ = 1.0, 100 centred ignition bubbles
Fi14_N150def	1	3D deflagration, $\rho_{c,9}$ = 2.9, 150 centred ignition bubbles
Fi14_N200def	1	3D deflagration, $\rho_{c,9}$ = 2.9, 200 centred ignition bubbles
Fi14_N300Cdef	1	3D deflagr., $\rho_{c,9}$ = 2.9, 300 compact centred ignition bubbles (highly sph. symmetry)
Fi14_N1600def	1	3D deflagration, $\rho_{c,9}$ = 2.9, 1600 centred ignition bubbles
Fi14_N1600Cdef	1	3D deflagration, $\rho_{c,9}$ = 2.9, 1600 compact centred ignition bubbles (highly sph. symmetry)
Iw99_W7	2	Deflagration, $\rho_{c,9}$ = 2.12, $Z_{\rm init}$ = 1$Z_\odot$
Iw99_W70	2	Deflagration, $\rho_{c,9}$ = 2.12, $Z_{\rm init}$ = 0$Z_\odot$
Iw99_WDD1	2	Delayed Detonation, $\rho_{c,9}$ = 2.12, $\rho_{T,7}$ = 1.7, $Z_{\rm init}$ = 1$Z_\odot$
Iw99_WDD2	2	Delayed Detonation, $\rho_{c,9}$ = 2.12, $\rho_{T,7}$ = 2.2, $Z_{\rm init}$ = 1$Z_\odot$
Iw99_WDD3	2	Delayed Detonation, $\rho_{c,9}$ = 2.12, $\rho_{T,7}$ = 3.0, $Z_{\rm init}$ = 1$Z_\odot$
Iw99_CDD1	2	Delayed Detonation, $\rho_{c,9}$ = 1.37, $\rho_{T,7}$ = 1.7, $Z_{\rm init}$ = 1$Z_\odot$
Iw99_CDD2	2	Delayed Detonation, $\rho_{c,9}$ = 1.37, $\rho_{T,7}$ = 2.2, $Z_{\rm init}$ = 1$Z_\odot$
Kr13_09_076	3	3D COWD-COWD violent merger, 0.9+0.76$M_\odot$, $Z_{\rm init}$ = 1$Z_\odot$
Kr15_N5_hybrid	4	3D Hybrid CONeWD deflagr. (CO core + ONe layers), off-centre deflagration, $\rho_{c,9}$ = 2.12
Kr16_09_076_Z0.01	3,5	3D COWD-COWD violent merger, 0.9+0.76$M_\odot$, $Z_{\rm init}$ = 0.01$Z_\odot$
Le18_050-1-c3-1P	6	2D Turbulent Deflagration, $\rho_{c,9}$ = 0.5, $Z_{\rm init}$ = 1$Z_\odot$, centred three-finger flame shape, C/O=1.0
Le18_100-1-c3-1P	6	2D Turbulent Deflagration, $\rho_{c,9}$ = 1.0, $Z_{\rm init}$ = 1$Z_\odot$, centred three-finger flame shape, C/O=1.0
Le18_100-0-c3	6	2D Deflagration-to-Detonation, $\rho_{c,9}$ = 1.0, $Z_{\rm init}$ = 0$Z_\odot$, centred three-finger flame shape
Le18_100-0.1-c3	6	2D Deflagration-to-Detonation, $\rho_{c,9}$ = 1.0, 0.1 $Z_{\rm init}$ = 1$Z_\odot$, centred three-finger flame shape
Le18_100-0.5-c3	6	2D Deflagration-to-Detonation, $\rho_{c,9}$ = 1.0, 0.5 $Z_{\rm init}$ = 1$Z_\odot$, centred three-finger flame shape
Le18_100-1-c3	6	2D Deflagration-to-Detonation, $\rho_{c,9}$ = 1.0, $Z_{\rm init}$ = 1$Z_\odot$, centred three-finger flame shape
Le18_100-2-c3	6	2D Deflagration-to-Detonation, $\rho_{c,9}$ = 1.0, 2.0 $Z_{\rm init}$ = 1$Z_\odot$, centred three-finger flame shape
Le18_100-3-c3	6	2D Deflagration-to-Detonation, $\rho_{c,9}$ = 1.0, 3.0 $Z_{\rm init}$ = 1$Z_\odot$, centred three-finger flame shape
Le18_100-5-c3	6	2D Deflagration-to-Detonation, $\rho_{c,9}$ = 1.0, 5.0 $Z_{\rm init}$ = 1$Z_\odot$, centred three-finger flame shape
Le18_300-1-c3-1P	6	2D Turbulent Deflagration, $\rho_{c,9}$ = 3.0, $Z_{\rm init}$ = 1$Z_\odot$, centred three-finger flame shape, C/O=1.0
Le18_300-0-c3	6	2D Deflagration-to-Detonation, $\rho_{c,9}$ = 3.0, $Z_{\rm init}$ = 0$Z_\odot$, centred three-finger flame shape
Le18_300-0.1-c3	6	2D Deflagration-to-Detonation, $\rho_{c,9}$ = 3.0, 0.1 $Z_{\rm init}$ = 1$Z_\odot$, centred three-finger flame shape
Le18_300-0.5-c3	6	2D Deflagration-to-Detonation, $\rho_{c,9}$ = 3.0, 0.5 $Z_{\rm init}$ = 1$Z_\odot$, centred three-finger flame shape
Le18_300-1-c3	6	2D Deflagration-to-Detonation, $\rho_{c,9}$ = 3.0, $Z_{\rm init}$ = 1$Z_\odot$, centred three-finger flame shape
Le18_300-2-c3	6	2D Deflagration-to-Detonation, $\rho_{c,9}$ = 3.0, 2.0 $Z_{\rm init}$ = 1$Z_\odot$, centred three-finger flame shape
Le18_300-3-c3	6	2D Deflagration-to-Detonation, $\rho_{c,9}$ = 3.0, 3.0 $Z_{\rm init}$ = 1$Z_\odot$, centred three-finger flame shape
Le18_300-5-c3	6	2D Deflagration-to-Detonation, $\rho_{c,9}$ = 3.0, 5.0 $Z_{\rm init}$ = 1$Z_\odot$, centred three-finger flame shape
Le18_500-1-c3-1P	6	2D Turbulent Deflagration, $\rho_{c,9}$ = 5.0, $Z_{\rm init}$ = 1$Z_\odot$, centred three-finger flame shape, C/O=1.0
Le18_500-0-c3	6	2D Deflagration-to-Detonation, $\rho_{c,9}$ = 5.0, $Z_{\rm init}$ = 0$Z_\odot$, centred three-finger flame shape
Le18_500-0.1-c3	6	2D Deflagration-to-Detonation, $\rho_{c,9}$ = 5.0, 0.1 $Z_{\rm init}$ = 1$Z_\odot$, centred three-finger flame shape
Le18_500-0.5-c3	6	2D Deflagration-to-Detonation, $\rho_{c,9}$ = 5.0, 0.5 $Z_{\rm init}$ = 1$Z_\odot$, centred three-finger flame shape
Le18_500-1-c3	6	2D Deflagration-to-Detonation, $\rho_{c,9}$ = 5.0, $Z_{\rm init}$ = 1$Z_\odot$, centred three-finger flame shape
Le18_500-2-c3	6	2D Deflagration-to-Detonation, $\rho_{c,9}$ = 5.0, 2.0 $Z_{\rm init}$ = 1$Z_\odot$, centred three-finger flame shape
Le18_500-3-c3	6	2D Deflagration-to-Detonation, $\rho_{c,9}$ = 5.0, 3.0 $Z_{\rm init}$ = 1$Z_\odot$, centred three-finger flame shape
Le18_500-5-c3	6	2D Deflagration-to-Detonation, $\rho_{c,9}$ = 5.0, 5.0 $Z_{\rm init}$ = 1$Z_\odot$, centred three-finger flame shape
Le20a_110_100_0_50	7	2D Double-Detonation, $M_{\rm WD}$ = 1.1, $M_{\rm He}$ = 1.0, $Z_{\rm init}$ = 0$Z_\odot$, type X
Le20a_110_100_02_50	7	2D Double-Detonation, $M_{\rm WD}$ = 1.1, $M_{\rm He}$ = 1.0, $Z_{\rm init}$ = 0.002$Z_\odot$
Le20a_110_100_1_50	7	2D Double-Detonation, $M_{\rm WD}$ = 1.1, $M_{\rm He}$ = 1.0, $Z_{\rm init}$ = 0.01$Z_\odot$
Le20a_110_100_2_50	7	2D Double-Detonation, $M_{\rm WD}$ = 1.1, $M_{\rm He}$ = 1.0, $Z_{\rm init}$ = 0.02$Z_\odot$, type X
Le20a_110_100_4_50	7	2D Double-Detonation, $M_{\rm WD}$ = 1.1, $M_{\rm He}$ = 1.0, $Z_{\rm init}$ = 0.04$Z_\odot$
Le20a_110_100_6_50	7	2D Double-Detonation, $M_{\rm WD}$ = 1.1, $M_{\rm He}$ = 1.0, $Z_{\rm init}$ = 0.06$Z_\odot$, type X
Le20a_110_100_10_50	7	2D Double-Detonation, $M_{\rm WD}$ = 1.1, $M_{\rm He}$ = 1.0, $Z_{\rm init}$ = 0.1$Z_\odot$, type X
Le20a_110_050_0_B50	7	2D Double-Detonation, $M_{\rm WD}$ = 1.1, $M_{\rm He}$ = 0.5, $Z_{\rm init}$ = 0$Z_\odot$, type Y
Le20a_110_050_02_B50	7	2D Double-Detonation, $M_{\rm WD}$ = 1.1, $M_{\rm He}$ = 0.5, $Z_{\rm init}$ = 0.002$Z_\odot$
Le20a_110_050_1_B50	7	2D Double-Detonation, $M_{\rm WD}$ = 1.1, $M_{\rm He}$ = 0.5, $Z_{\rm init}$ = 0.01$Z_\odot$
Le20a_110_050_2_B50	7	2D Double-Detonation, $M_{\rm WD}$ = 1.1, $M_{\rm He}$ = 0.5, $Z_{\rm init}$ = 0.02$Z_\odot$, type Y

Table 1 – *continued* A table continued from the previous one.

Model Name	Ref.	Basic Proprieties
Le20a_110_050_4_B50	7	2D Double-Detonation, $M_{\rm WD}$ = 1.1, $M_{\rm He}$ = 0.5, $Z_{\rm init}$ = 0.04$Z_{\odot}$
Le20a_110_050_6_B50	7	2D Double-Detonation, $M_{\rm WD}$ = 1.1, $M_{\rm He}$ = 0.5, $Z_{\rm init}$ = 0.06$Z_{\odot}$, type Y
Le20a_110_050_10_B50	7	2D Double-Detonation, $M_{\rm WD}$ = 1.1, $M_{\rm He}$ = 0.5, $Z_{\rm init}$ = 0.1$Z_{\odot}$, type Y
Le20a_100_050_0_S50	7	2D Double-Detonation, $M_{\rm WD}$ = 1.0, $M_{\rm He}$ = 0.5, $Z_{\rm init}$ = 0$Z_{\odot}$
Le20a_100_050_02_S50	7	2D Double-Detonation, $M_{\rm WD}$ = 1.1, $M_{\rm He}$ = 0.5, $Z_{\rm init}$ = 0.002$Z_{\odot}$
Le20a_100_050_1_S50	7	2D Double-Detonation, $M_{\rm WD}$ = 1.1, $M_{\rm He}$ = 0.5, $Z_{\rm init}$ = 0.01$Z_{\odot}$
Le20a_100_050_2_S50	7	2D Double-Detonation, $M_{\rm WD}$ = 1.1, $M_{\rm He}$ = 0.5, $Z_{\rm init}$ = 0.02$Z_{\odot}$, type S
Le20a_100_050_4_S50	7	2D Double-Detonation, $M_{\rm WD}$ = 1.1, $M_{\rm He}$ = 0.5, $Z_{\rm init}$ = 0.04$Z_{\odot}$
Le20a_100_050_6_S50	7	2D Double-Detonation, $M_{\rm WD}$ = 1.1, $M_{\rm He}$ = 0.5, $Z_{\rm init}$ = 0.06$Z_{\odot}$
Le20a_100_050_10_S50	7	2D Double-Detonation, $M_{\rm WD}$ = 1.1, $M_{\rm He}$ = 0.5, $Z_{\rm init}$ = 0.1$Z_{\odot}$
Le20a_090_150_2_50	7	2D Double-Detonation, $M_{\rm WD}$ = 0.9, $M_{\rm He}$ = 1.5, $Z_{\rm init}$ = 0.02$Z_{\odot}$, type Y
Le20a_095_150_2_50	7	2D Double-Detonation, $M_{\rm WD}$ = 0.95, $M_{\rm He}$ = 1.5, $Z_{\rm init}$ = 0.02$Z_{\odot}$, type X
Le20a_100_100_2_50	7	2D Double-Detonation, $M_{\rm WD}$ = 1.0, $M_{\rm He}$ = 1.0, $Z_{\rm init}$ = 0.02$Z_{\odot}$, type N
Le20a_105_100_2_50	7	2D Double-Detonation, $M_{\rm WD}$ = 1.05, $M_{\rm He}$ = 1.0, $Z_{\rm init}$ = 0.02$Z_{\odot}$, type X
Le20a_115_100_2_50	7	2D Double-Detonation, $M_{\rm WD}$ = 1.15, $M_{\rm He}$ = 1.0, $Z_{\rm init}$ = 0.02$Z_{\odot}$, type D
Le20a_120_050_2_50	7	2D Double-Detonation, $M_{\rm WD}$ = 1.2, $M_{\rm He}$ = 0.5, $Z_{\rm init}$ = 0.02$Z_{\odot}$, type X
Le20a_090_050_2_B50	7	2D Double-Detonation, $M_{\rm WD}$ = 0.9, $M_{\rm He}$ = 0.5, $Z_{\rm init}$ = 0.02$Z_{\odot}$, type Y
Le20a_095_050_2_B50	7	2D Double-Detonation, $M_{\rm WD}$ = 0.95, $M_{\rm He}$ = 0.5, $Z_{\rm init}$ = 0.02$Z_{\odot}$, type Y
Le20a_100_050_2_B50	7	2D Double-Detonation, $M_{\rm WD}$ = 1.0, $M_{\rm He}$ = 0.5, $Z_{\rm init}$ = 0.02$Z_{\odot}$, type Y
Le20a_105_050_2_B50	7	2D Double-Detonation, $M_{\rm WD}$ = 1.05, $M_{\rm He}$ = 0.5, $Z_{\rm init}$ = 0.02$Z_{\odot}$, type Y
Le20a_120_050_2_B50	7	2D Double-Detonation, $M_{\rm WD}$ = 1.2, $M_{\rm He}$ = 0.5, $Z_{\rm init}$ = 0.02$Z_{\odot}$
Le20a_090_050_2_S50	7	2D Double-Detonation, $M_{\rm WD}$ = 0.9, $M_{\rm He}$ = 0.5, $Z_{\rm init}$ = 0.02$Z_{\odot}$, type S
Le20a_095_050_2_S50	7	2D Double-Detonation, $M_{\rm WD}$ = 0.95, $M_{\rm He}$ = 0.5, $Z_{\rm init}$ = 0.02$Z_{\odot}$, type S
Le20a_100_050_2_S50	7	2D Double-Detonation, $M_{\rm WD}$ = 1.0, $M_{\rm He}$ = 0.5, $Z_{\rm init}$ = 0.02$Z_{\odot}$, type S
Le20a_105_050_2_S50	7	2D Double-Detonation, $M_{\rm WD}$ = 1.05, $M_{\rm He}$ = 0.5, $Z_{\rm init}$ = 0.02$Z_{\odot}$, type S
Le20a_120_050_2_S50	7	2D Double-Detonation, $M_{\rm WD}$ = 1.2, $M_{\rm He}$ = 0.5, $Z_{\rm init}$ = 0.02$Z_{\odot}$
Le20b_CO_100_133_1_c3_1	8	2D Turbulent Deflagration, $\rho_{c,9}$ = 1.0, $M_{\rm CO}$ = 1.33, centred three-finger flame shape, C/O=1
Le20b_CO_200_135_1_c3_1	8	2D Turbulent Deflagration, $\rho_{c,9}$ = 2.0, $M_{\rm CO}$ = 1.35, centred three-finger flame shape, C/O=1
Le20b_CO_300_137_1_c3_1	8	2D Turbulent Deflagration, $\rho_{c,9}$ = 3.0, $M_{\rm CO}$ = 1.37, centred three-finger flame shape, C/O=1
Le20b_CO_500_138_1_c3_1	8	2D Turbulent Deflagration, $\rho_{c,9}$ = 5.0, $M_{\rm CO}$ = 1.38, centred three-finger flame shape, C/O=1
Le20b_CO_550_138_1_c3_1	8	2D Turbulent Deflagration, $\rho_{c,9}$ = 5.5, $M_{\rm CO}$ = 1.38, centred three-finger flame shape, C/O=1
Le20b_CO_750_139_1_c3_1	8	2D Turbulent Deflagration, $\rho_{c,9}$ = 7.0, $M_{\rm CO}$ = 1.39, centred three-finger flame shape, C/O=1
Le20b_CO_900_140_1_c3_1	8	2D Turbulent Deflagration, $\rho_{c,9}$ = 9.0, $M_{\rm CO}$ = 1.4, centred three-finger flame shape, C/O=1
Le20b_CONe_100_043_1_c3	8	2D Hybrid CONeWD Deflagration (CO core + ONeMg layer), $\rho_{c,9}$ = 1.0, $M_{\rm CO}$ = 0.43
Le20b_CONe_200_045_1_c3	8	2D Hybrid CONeWD Deflagration (CO core + ONeMg layer), $\rho_{c,9}$ = 2.0, $M_{\rm CO}$ = 0.45
Le20b_CONe_300_047_1_c3	8	2D Hybrid CONeWD Deflagration (CO core + ONeMg layer), $\rho_{c,9}$ = 3.0, $M_{\rm CO}$ = 0.47
Le20b_CONe_500_048_1_c3	8	2D Hybrid CONeWD Deflagration (CO core + ONeMg layer), $\rho_{c,9}$ = 5.0, $M_{\rm CO}$ = 0.48
Le20b_CONe_550_048_1_c3	8	2D Hybrid CONeWD Deflagration (CO core + ONeMg layer), $\rho_{c,9}$ = 5.5, $M_{\rm CO}$ = 0.48
Le20b_CONe_750_049_1_c3	8	2D Hybrid CONeWD Deflagration (CO core + ONeMg layer), $\rho_{c,9}$ = 7.5, $M_{\rm CO}$ = 0.49
Le20b_CONe_900_050_1_c3	8	2D Hybrid CONeWD Deflagration (CO core + ONeMg layer), $\rho_{c,9}$ = 9.0, $M_{\rm CO}$ = 0.5
Ma10_C-DEF	9	2D Deflagration, $\rho_{c,9}$ = 2.9, centred ignition
Ma10_C-DDT	9	2D Delayed-Detonation, $\rho_{c,9}$ = 2.9, $\rho_{\rm T,7} \leq 1.0$, centred ignition
Ma10_O-DDT	9	2D Delayed-Detonation, $\rho_{c,9}$ = 2.9, $\rho_{\rm T,7} \leq 1.0$, off-centre ignition
Ma15_CO15e7	10	3D COWD Delayed-Detonation, $M_{\rm WD}$ = 1.23, $\rho_{c,9}$ = 0.15, C/O=1
Ma15_ONe10e7	10	3D ONeWD Delayed-Detonation, $M_{\rm WD}$ = 1.18, $\rho_{c,9}$ = 0.1
Ma15_ONe13e7	10	3D ONeWD Delayed-Detonation, $M_{\rm WD}$ = 1.21, $\rho_{c,9}$ = 0.13
Ma15_ONe15e7	10	3D ONeWD Delayed-Detonation, $M_{\rm WD}$ = 1.23, $\rho_{c,9}$ = 0.15
Ma15_ONe17e7	10	3D ONeWD Delayed-Detonation, $M_{\rm WD}$ = 1.24, $\rho_{c,9}$ = 0.17
Ma15_ONe20e7	10	3D ONeWD Delayed-Detonation, $M_{\rm WD}$ = 1.25, $\rho_{c,9}$ = 0.2
Oh14_DDT8_N100_c50	11	Se13_N100, Homogeneous WD with 50% carbon mass fraction
Oh14_DDT8_N100_rpc20	11	Se13_N100, Carbon depleted core WD with 20% carbon mass fraction
Oh14_DDT8_N100_rpc32	11	Se13_N100, Carbon depleted core WD with 32% carbon mass fraction
Oh14_DDT8_N100_rpc40	11	Se13_N100, Carbon depleted core WD with 40% carbon mass fraction
Pa10_09_09	12	WD+WD violent merger, 1.1+0.9 $M_{\odot}$, $\rho_{c,9} = 1.4 \times 10^{-2}$
Pa12_11_09	13	WD+WD violent merger, 1.1+0.9 $M_{\odot}$, $Z_{\rm init} = Z_{\odot}$
Pa16_1A	14	WD+WD collision, 0.6+0.6 $M_{\odot}$, $\rho_{c,9} = 3.4 \times 10^{-3}$
Pa16_1C	14	WD+WD w/ He shell collision, 0.6+0.6 $M_{\odot}$, $M_{\rm He} = 0.01 M_{\odot}$, $\rho_{c,9} = 3.4 \times 10^{-3}$
Se13_N1	15	3D Delayed-Detonation, $\rho_{c,9}$ = 2.9, 1 centred ignition spot
Se13_N3	15	3D Delayed-Detonation, $\rho_{c,9}$ = 2.9, 3 centred ignition spots

Table 1 – *continued* A table continued from the previous one.

Model Name	Ref.	Basic Proprieties
Se13_N5	15	3D Delayed-Detonation, $\rho_{c,9}$ = 2.9, 5 centred ignition spots
Se13_N10	15	3D Delayed-Detonation, $\rho_{c,9}$ = 2.9, 10 centred ignition spots
Se13_N20	15	3D Delayed-Detonation, $\rho_{c,9}$ = 2.9, 20 centred ignition spots
Se13_N40	15	3D Delayed-Detonation, $\rho_{c,9}$ = 2.9, 40 centred ignition spots
Se13_N100H	15	3D Delayed-Detonation, $\rho_{c,9}$ = 5.5, 100 centred ignition spots
Se13_N100	15	3D Delayed-Detonation, $\rho_{c,9}$ = 2.9, 100 centred ignition spots
Se13_N100L	15	3D Delayed-Detonation, $\rho_{c,9}$ = 1.0, 100 centred ignition spots
Se13_N150	15	3D Delayed-Detonation, $\rho_{c,9}$ = 2.9, 150 centred ignition spots
Se13_N200	15	3D Delayed-Detonation, $\rho_{c,9}$ = 2.9, 200 centred ignition spots
Se13_N300C	15	3D Delayed-Detonation, $\rho_{c,9}$ = 2.9, 300 compact centred ignition bubble, highly sph. symmetry
Se13_N1600	15	3D Delayed-Detonation, $\rho_{c,9}$ = 2.9, 1600 centred ignition spots
Se13_N1600C	15	3D Delayed-Detonation, $\rho_{c,9}$ = 2.9, 1600 compact centred ignition bubble, highly sph. symmetry
Se13_N100_Z0.5	15	3D Delayed-Detonation, $\rho_{c,9}$ = 2.9, 100 centred ignition spots, $Z_{\rm init} = 0.5 Z_\odot$
Se13_N100_Z0.1	15	3D Delayed-Detonation, $\rho_{c,9}$ = 2.9, 100 centred ignition spots, $Z_{\rm init} = 0.1 Z_\odot$
Se13_N100_Z0.01	15	3D Delayed-Detonation, $\rho_{c,9}$ = 2.9, 100 centred ignition spots, $Z_{\rm init} = 0.01 Z_\odot$
Se16_GCD200	16	3D Gravitationally confined detonation, $\rho_{c,9}$ = 2.9, one ignition spot with off-centred distance from the center of the ignition kernel to the center of WD of 200km
Sh18_08_3070_Z005_01	17	1D Dynamically-driven double-degen. double-deton., $M_{\rm WD}$ = 0.8, C/O=30/70, $Z_{\rm init}$ = 0.005, $f_{^{12}C+^{16}O}$ = 0.1
Sh18_08_3070_Z005_1	17	1D Dynamically-driven double-degen. double-deton., $M_{\rm WD}$ = 0.8, C/O=30/70, $Z_{\rm init}$ = 0.005, $f_{^{12}C+^{16}O}$ = 1.0
Sh18_08_3070_Z01_01	17	1D Dynamically-driven double-degen. double-deton., $M_{\rm WD}$ = 0.8, C/O=30/70, $Z_{\rm init}$ = 0.01, $f_{^{12}C+^{16}O}$ = 0.1
Sh18_08_3070_Z01_1	17	1D Dynamically-driven double-degen. double-deton., $M_{\rm WD}$ = 0.8, C/O=30/70, $Z_{\rm init}$ = 0.01, $f_{^{12}C+^{16}O}$ = 1.0
Sh18_08_3070_Z0_01	17	1D Dynamically-driven double-degen. double-deton., $M_{\rm WD}$ = 0.8, C/O=30/70, $Z_{\rm init}$ = 0.00, $f_{^{12}C+^{16}O}$ = 0.1
Sh18_08_3070_Z02_01	17	1D Dynamically-driven double-degen. double-deton., $M_{\rm WD}$ = 0.8, C/O=30/70, $Z_{\rm init}$ = 0.02, $f_{^{12}C+^{16}O}$ = 1.0
Sh18_08_3070_Z02_1	17	1D Dynamically-driven double-degen. double-deton., $M_{\rm WD}$ = 0.8, C/O=30/70, $Z_{\rm init}$ = 0.02, $f_{^{12}C+^{16}O}$ = 0.1
Sh18_08_3070_Z0_1	17	1D Dynamically-driven double-degen. double-deton., $M_{\rm WD}$ = 0.8, C/O=30/70, $Z_{\rm init}$ = 0.00, $f_{^{12}C+^{16}O}$ = 1.0
Sh18_08_5050_Z005_01	17	1D Dynamically-driven double-degen. double-deton., $M_{\rm WD}$ = 0.8, C/O=50/50, $Z_{\rm init}$ = 0.005, $f_{^{12}C+^{16}O}$ = 0.1
Sh18_08_5050_Z005_1	17	1D Dynamically-driven double-degen. double-deton., $M_{\rm WD}$ = 0.8, C/O=50/50, $Z_{\rm init}$ = 0.005, $f_{^{12}C+^{16}O}$ = 1.0
Sh18_08_5050_Z01_01	17	1D Dynamically-driven double-degen. double-deton., $M_{\rm WD}$ = 0.8, C/O=50/50, $Z_{\rm init}$ = 0.01, $f_{^{12}C+^{16}O}$ = 0.1
Sh18_08_5050_Z01_1	17	1D Dynamically-driven double-degen. double-deton., $M_{\rm WD}$ = 0.8, C/O=50/50, $Z_{\rm init}$ = 0.01, $f_{^{12}C+^{16}O}$ = 1.0
Sh18_08_5050_Z0_01	17	1D Dynamically-driven double-degen. double-deton., $M_{\rm WD}$ = 0.8, C/O=50/50, $Z_{\rm init}$ = 0.00, $f_{^{12}C+^{16}O}$ = 0.1
Sh18_08_5050_Z02_01	17	1D Dynamically-driven double-degen. double-deton., $M_{\rm WD}$ = 0.8, C/O=50/50, $Z_{\rm init}$ = 0.02, $f_{^{12}C+^{16}O}$ = 1.0
Sh18_08_5050_Z02_1	17	1D Dynamically-driven double-degen. double-deton., $M_{\rm WD}$ = 0.8, C/O=50/50, $Z_{\rm init}$ = 0.02, $f_{^{12}C+^{16}O}$ = 0.1
Sh18_08_5050_Z0_1	17	1D Dynamically-driven double-degen. double-deton., $M_{\rm WD}$ = 0.8, C/O=50/50, $Z_{\rm init}$ = 0.00, $f_{^{12}C+^{16}O}$ = 1.0
Sh18_085_3070_Z005_01	17	1D Dynamically-driven double-degen. double-deton., $M_{\rm WD}$ = 0.85, C/O=30/70, $Z_{\rm init}$ = 0.005, $f_{^{12}C+^{16}O}$ = 0.1
Sh18_085_3070_Z005_1	17	1D Dynamically-driven double-degen. double-deton., $M_{\rm WD}$ = 0.85, C/O=30/70, $Z_{\rm init}$ = 0.005, $f_{^{12}C+^{16}O}$ = 1.0
Sh18_085_3070_Z01_01	17	1D Dynamically-driven double-degen. double-deton., $M_{\rm WD}$ = 0.85, C/O=30/70, $Z_{\rm init}$ = 0.01, $f_{^{12}C+^{16}O}$ = 0.1
Sh18_085_3070_Z01_1	17	1D Dynamically-driven double-degen. double-deton., $M_{\rm WD}$ = 0.85, C/O=30/70, $Z_{\rm init}$ = 0.01, $f_{^{12}C+^{16}O}$ = 1.0
Sh18_085_3070_Z0_01	17	1D Dynamically-driven double-degen. double-deton., $M_{\rm WD}$ = 0.85, C/O=30/70, $Z_{\rm init}$ = 0.00, $f_{^{12}C+^{16}O}$ = 0.1
Sh18_085_3070_Z02_01	17	1D Dynamically-driven double-degen. double-deton., $M_{\rm WD}$ = 0.85, C/O=30/70, $Z_{\rm init}$ = 0.02, $f_{^{12}C+^{16}O}$ = 1.0
Sh18_085_3070_Z02_1	17	1D Dynamically-driven double-degen. double-deton., $M_{\rm WD}$ = 0.85, C/O=30/70, $Z_{\rm init}$ = 0.02, $f_{^{12}C+^{16}O}$ = 0.1
Sh18_085_3070_Z0_1	17	1D Dynamically-driven double-degen. double-deton., $M_{\rm WD}$ = 0.85, C/O=30/70, $Z_{\rm init}$ = 0.00, $f_{^{12}C+^{16}O}$ = 1.0
Sh18_085_5050_Z005_01	17	1D Dynamically-driven double-degen. double-deton., $M_{\rm WD}$ = 0.85, C/O=50/50, $Z_{\rm init}$ = 0.005, $f_{^{12}C+^{16}O}$ = 0.1
Sh18_085_5050_Z005_1	17	1D Dynamically-driven double-degen. double-deton., $M_{\rm WD}$ = 0.85, C/O=50/50, $Z_{\rm init}$ = 0.005, $f_{^{12}C+^{16}O}$ = 1.0
Sh18_085_5050_Z01_01	17	1D Dynamically-driven double-degen. double-deton., $M_{\rm WD}$ = 0.85, C/O=50/50, $Z_{\rm init}$ = 0.01, $f_{^{12}C+^{16}O}$ = 0.1
Sh18_085_5050_Z01_1	17	1D Dynamically-driven double-degen. double-deton., $M_{\rm WD}$ = 0.85, C/O=50/50, $Z_{\rm init}$ = 0.01, $f_{^{12}C+^{16}O}$ = 1.0
Sh18_085_5050_Z0_01	17	1D Dynamically-driven double-degen. double-deton., $M_{\rm WD}$ = 0.85, C/O=50/50, $Z_{\rm init}$ = 0.00, $f_{^{12}C+^{16}O}$ = 0.1
Sh18_085_5050_Z02_01	17	1D Dynamically-driven double-degen. double-deton., $M_{\rm WD}$ = 0.85, C/O=50/50, $Z_{\rm init}$ = 0.02, $f_{^{12}C+^{16}O}$ = 1.0
Sh18_085_5050_Z02_1	17	1D Dynamically-driven double-degen. double-deton., $M_{\rm WD}$ = 0.85, C/O=50/50, $Z_{\rm init}$ = 0.02, $f_{^{12}C+^{16}O}$ = 0.1
Sh18_085_5050_Z0_1	17	1D Dynamically-driven double-degen. double-deton., $M_{\rm WD}$ = 0.85, C/O=50/50, $Z_{\rm init}$ = 0.00, $f_{^{12}C+^{16}O}$ = 1.0
Sh18_090_3070_Z005_01	17	1D Dynamically-driven double-degen. double-deton., $M_{\rm WD}$ = 0.9, C/O=30/70, $Z_{\rm init}$ = 0.005, $f_{^{12}C+^{16}O}$ = 0.1
Sh18_090_3070_Z005_1	17	1D Dynamically-driven double-degen. double-deton., $M_{\rm WD}$ = 0.9, C/O=30/70, $Z_{\rm init}$ = 0.005, $f_{^{12}C+^{16}O}$ = 1.0
Sh18_090_3070_Z01_01	17	1D Dynamically-driven double-degen. double-deton., $M_{\rm WD}$ = 0.9, C/O=30/70, $Z_{\rm init}$ = 0.01, $f_{^{12}C+^{16}O}$ = 0.1
Sh18_090_3070_Z01_1	17	1D Dynamically-driven double-degen. double-deton., $M_{\rm WD}$ = 0.9, C/O=30/70, $Z_{\rm init}$ = 0.01, $f_{^{12}C+^{16}O}$ = 1.0
Sh18_090_3070_Z0_01	17	1D Dynamically-driven double-degen. double-deton., $M_{\rm WD}$ = 0.9, C/O=30/70, $Z_{\rm init}$ = 0.00, $f_{^{12}C+^{16}O}$ = 0.1
Sh18_090_3070_Z02_01	17	1D Dynamically-driven double-degen. double-deton., $M_{\rm WD}$ = 0.9, C/O=30/70, $Z_{\rm init}$ = 0.02, $f_{^{12}C+^{16}O}$ = 1.0
Sh18_090_3070_Z02_1	17	1D Dynamically-driven double-degen. double-deton., $M_{\rm WD}$ = 0.9, C/O=30/70, $Z_{\rm init}$ = 0.02, $f_{^{12}C+^{16}O}$ = 0.1
Sh18_090_3070_Z0_1	17	1D Dynamically-driven double-degen. double-deton., $M_{\rm WD}$ = 0.9, C/O=30/70, $Z_{\rm init}$ = 0.00, $f_{^{12}C+^{16}O}$ = 1.0
Sh18_090_5050_Z005_01	17	1D Dynamically-driven double-degen. double-deton., $M_{\rm WD}$ = 0.9, C/O=50/50, $Z_{\rm init}$ = 0.005, $f_{^{12}C+^{16}O}$ = 0.1
Sh18_090_5050_Z005_1	17	1D Dynamically-driven double-degen. double-deton., $M_{\rm WD}$ = 0.9, C/O=50/50, $Z_{\rm init}$ = 0.005, $f_{^{12}C+^{16}O}$ = 1.0
Sh18_090_5050_Z01_01	17	1D Dynamically-driven double-degen. double-deton., $M_{\rm WD}$ = 0.9, C/O=50/50, $Z_{\rm init}$ = 0.01, $f_{^{12}C+^{16}O}$ = 0.1
Sh18_090_5050_Z01_1	17	1D Dynamically-driven double-degen. double-deton., $M_{\rm WD}$ = 0.9, C/O=50/50, $Z_{\rm init}$ = 0.01, $f_{^{12}C+^{16}O}$ = 1.0
Sh18_090_5050_Z0_01	17	1D Dynamically-driven double-degen. double-deton., $M_{\rm WD}$ = 0.9, C/O=50/50, $Z_{\rm init}$ = 0.00, $f_{^{12}C+^{16}O}$ = 0.1

Table 1 – *continued* A table continued from the previous one.

Model Name	Ref.	Basic Proprieties
Sh18_090_5050_Z02_01	17	1D Dynamically-driven double-degen. double-deton., $M_{\rm WD}$ = 0.9, C/O=50/50, $Z_{\rm init}$ = 0.02, $f_{^{12}C+^{16}O}$ = 1.0
Sh18_090_5050_Z02_1	17	1D Dynamically-driven double-degen. double-deton., $M_{\rm WD}$ = 0.9, C/O=50/50, $Z_{\rm init}$ = 0.02, $f_{^{12}C+^{16}O}$ = 0.1
Sh18_090_5050_Z0_1	17	1D Dynamically-driven double-degen. double-deton., $M_{\rm WD}$ = 0.9, C/O=50/50, $Z_{\rm init}$ = 0.00, $f_{^{12}C+^{16}O}$ = 1.0
Sh18_10_3070_Z005_01	17	1D Dynamically-driven double-degen. double-deton., $M_{\rm WD}$ = 1.0, C/O=30/70, $Z_{\rm init}$ = 0.005, $f_{^{12}C+^{16}O}$ = 0.1
Sh18_10_3070_Z005_1	17	1D Dynamically-driven double-degen. double-deton., $M_{\rm WD}$ = 1.0, C/O=30/70, $Z_{\rm init}$ = 0.005, $f_{^{12}C+^{16}O}$ = 1.0
Sh18_10_3070_Z01_01	17	1D Dynamically-driven double-degen. double-deton., $M_{\rm WD}$ = 1.0, C/O=30/70, $Z_{\rm init}$ = 0.01, $f_{^{12}C+^{16}O}$ = 0.1
Sh18_10_3070_Z01_1	17	1D Dynamically-driven double-degen. double-deton., $M_{\rm WD}$ = 1.0, C/O=30/70, $Z_{\rm init}$ = 0.01, $f_{^{12}C+^{16}O}$ = 1.0
Sh18_10_3070_Z0_01	17	1D Dynamically-driven double-degen. double-deton., $M_{\rm WD}$ = 1.0, C/O=30/70, $Z_{\rm init}$ = 0.00, $f_{^{12}C+^{16}O}$ = 0.1
Sh18_10_3070_Z02_01	17	1D Dynamically-driven double-degen. double-deton., $M_{\rm WD}$ = 1.0, C/O=30/70, $Z_{\rm init}$ = 0.02, $f_{^{12}C+^{16}O}$ = 1.0
Sh18_10_3070_Z02_1	17	1D Dynamically-driven double-degen. double-deton., $M_{\rm WD}$ = 1.0, C/O=30/70, $Z_{\rm init}$ = 0.02, $f_{^{12}C+^{16}O}$ = 0.1
Sh18_10_3070_Z0_1	17	1D Dynamically-driven double-degen. double-deton., $M_{\rm WD}$ = 1.0, C/O=30/70, $Z_{\rm init}$ = 0.00, $f_{^{12}C+^{16}O}$ = 1.0
Sh18_10_5050_Z005_01	17	1D Dynamically-driven double-degen. double-deton., $M_{\rm WD}$ = 1.0, C/O=50/50, $Z_{\rm init}$ = 0.005, $f_{^{12}C+^{16}O}$ = 0.1
Sh18_10_5050_Z005_1	17	1D Dynamically-driven double-degen. double-deton., $M_{\rm WD}$ = 1.0, C/O=50/50, $Z_{\rm init}$ = 0.005, $f_{^{12}C+^{16}O}$ = 1.0
Sh18_10_5050_Z01_01	17	1D Dynamically-driven double-degen. double-deton., $M_{\rm WD}$ = 1.0, C/O=50/50, $Z_{\rm init}$ = 0.01, $f_{^{12}C+^{16}O}$ = 0.1
Sh18_10_5050_Z01_1	17	1D Dynamically-driven double-degen. double-deton., $M_{\rm WD}$ = 1.0, C/O=50/50, $Z_{\rm init}$ = 0.01, $f_{^{12}C+^{16}O}$ = 1.0
Sh18_10_5050_Z0_01	17	1D Dynamically-driven double-degen. double-deton., $M_{\rm WD}$ = 1.0, C/O=50/50, $Z_{\rm init}$ = 0.00, $f_{^{12}C+^{16}O}$ = 0.1
Sh18_10_5050_Z02_01	17	1D Dynamically-driven double-degen. double-deton., $M_{\rm WD}$ = 1.0, C/O=50/50, $Z_{\rm init}$ = 0.02, $f_{^{12}C+^{16}O}$ = 1.0
Sh18_10_5050_Z02_1	17	1D Dynamically-driven double-degen. double-deton., $M_{\rm WD}$ = 1.0, C/O=50/50, $Z_{\rm init}$ = 0.02, $f_{^{12}C+^{16}O}$ = 0.1
Sh18_10_5050_Z0_1	17	1D Dynamically-driven double-degen. double-deton., $M_{\rm WD}$ = 1.0, C/O=50/50, $Z_{\rm init}$ = 0.00, $f_{^{12}C+^{16}O}$ = 1.0
Sh18_11_3070_Z005_01	17	1D Dynamically-driven double-degen. double-deton., $M_{\rm WD}$ = 1.1, C/O=30/70, $Z_{\rm init}$ = 0.005, $f_{^{12}C+^{16}O}$ = 0.1
Sh18_11_3070_Z005_1	17	1D Dynamically-driven double-degen. double-deton., $M_{\rm WD}$ = 1.1, C/O=30/70, $Z_{\rm init}$ = 0.005, $f_{^{12}C+^{16}O}$ = 1.0
Sh18_11_3070_Z01_01	17	1D Dynamically-driven double-degen. double-deton., $M_{\rm WD}$ = 1.1, C/O=30/70, $Z_{\rm init}$ = 0.01, $f_{^{12}C+^{16}O}$ = 0.1
Sh18_11_3070_Z01_1	17	1D Dynamically-driven double-degen. double-deton., $M_{\rm WD}$ = 1.1, C/O=30/70, $Z_{\rm init}$ = 0.01, $f_{^{12}C+^{16}O}$ = 1.0
Sh18_11_3070_Z0_01	17	1D Dynamically-driven double-degen. double-deton., $M_{\rm WD}$ = 1.1, C/O=30/70, $Z_{\rm init}$ = 0.00, $f_{^{12}C+^{16}O}$ = 0.1
Sh18_11_3070_Z02_01	17	1D Dynamically-driven double-degen. double-deton., $M_{\rm WD}$ = 1.1, C/O=30/70, $Z_{\rm init}$ = 0.02, $f_{^{12}C+^{16}O}$ = 1.0
Sh18_11_3070_Z02_1	17	1D Dynamically-driven double-degen. double-deton., $M_{\rm WD}$ = 1.1, C/O=30/70, $Z_{\rm init}$ = 0.02, $f_{^{12}C+^{16}O}$ = 0.1
Sh18_11_3070_Z0_1	17	1D Dynamically-driven double-degen. double-deton., $M_{\rm WD}$ = 1.1, C/O=30/70, $Z_{\rm init}$ = 0.00, $f_{^{12}C+^{16}O}$ = 1.0
Sh18_11_5050_Z005_01	17	1D Dynamically-driven double-degen. double-deton., $M_{\rm WD}$ = 1.1, C/O=50/50, $Z_{\rm init}$ = 0.005, $f_{^{12}C+^{16}O}$ = 0.1
Sh18_11_5050_Z005_1	17	1D Dynamically-driven double-degen. double-deton., $M_{\rm WD}$ = 1.1, C/O=50/50, $Z_{\rm init}$ = 0.005, $f_{^{12}C+^{16}O}$ = 1.0
Sh18_11_5050_Z01_01	17	1D Dynamically-driven double-degen. double-deton., $M_{\rm WD}$ = 1.1, C/O=50/50, $Z_{\rm init}$ = 0.01, $f_{^{12}C+^{16}O}$ = 0.1
Sh18_11_5050_Z01_1	17	1D Dynamically-driven double-degen. double-deton., $M_{\rm WD}$ = 1.1, C/O=50/50, $Z_{\rm init}$ = 0.01, $f_{^{12}C+^{16}O}$ = 1.0
Sh18_11_5050_Z0_01	17	1D Dynamically-driven double-degen. double-deton., $M_{\rm WD}$ = 1.1, C/O=50/50, $Z_{\rm init}$ = 0.00, $f_{^{12}C+^{16}O}$ = 0.1
Sh18_11_5050_Z02_01	17	1D Dynamically-driven double-degen. double-deton., $M_{\rm WD}$ = 1.1, C/O=50/50, $Z_{\rm init}$ = 0.02, $f_{^{12}C+^{16}O}$ = 1.0
Sh18_11_5050_Z02_1	17	1D Dynamically-driven double-degen. double-deton., $M_{\rm WD}$ = 1.1, C/O=50/50, $Z_{\rm init}$ = 0.02, $f_{^{12}C+^{16}O}$ = 0.1
Sh18_11_5050_Z0_1	17	1D Dynamically-driven double-degen. double-deton., $M_{\rm WD}$ = 1.1, C/O=50/50, $Z_{\rm init}$ = 0.00, $f_{^{12}C+^{16}O}$ = 1.0
Si10_det_0.81	18	1D Detonation in Sub-Ch mass CO WD, $M_{\rm WD}$ = 0.81, $\rho_{c,7}$ = 7.9, C/O/Ne = 50/50/0
Si10_det_0.88	18	1D Detonation in Sub-Ch mass CO WD, $M_{\rm WD}$ = 0.88, $\rho_{c,7}$ = 4.15, C/O/Ne = 50/50/0
Si10_det_0.97	18	1D Detonation in Sub-Ch mass CO WD, $M_{\rm WD}$ = 0.97, $\rho_{c,7}$ = 4.15, C/O/Ne = 50/50/0
Si10_det_1.06	18	1D Detonation in Sub-Ch mass CO WD, $M_{\rm WD}$ = 1.06, $\rho_{c,7}$ = 2.4, C/O/Ne = 50/50/0
Si10_det_1.06_0.075Ne	18	1D Detonation in Sub-Ch mass CO WD, $M_{\rm WD}$ = 1.06, $\rho_{c,7}$ = 1.45, C/O/Ne = 42.5/50/7.5
Si10_det_1.15	18	1D Detonation in Sub-Ch mass CO WD, $M_{\rm WD}$ = 1.15, $\rho_{c,7}$ = 1.0, C/O/Ne = 50/50/0
Si12_CSDD-L	19	2D Converging-shock double-detonation (low-mass), $M_{\rm CO}$ = 0.45, $\rho_{c,9} = 3.81 \times 10^{-3}$
Si12_CSDD-S	19	2D Converging-shock double-detonation (standard), $M_{\rm CO}$ = 0.58, $\rho_{c,9} = 8.5 \times 10^{-3}$
Si12_ELDD-L	19	2D Edge-lit double-detonation (low-mass), $M_{\rm CO}$ = 0.45, $\rho_{c,9} = 3.81 \times 10^{-3}$
Si12_ELDD-S	19	2D Edge-lit double-detonation (standard), $M_{\rm CO}$ = 0.58, $\rho_{c,9} = 8.5 \times 10^{-3}$
Si12_HeD-L	19	2D He-only Detonation (low-mass), $M_{\rm CO}$ = 0.45, $\rho_{c,9} = 3.81 \times 10^{-3}$
Si12_HeD-S	19	2D He-only Detonation (standard), $M_{\rm CO}$ = 0.58, $\rho_{c,9} = 8.5 \times 10^{-3}$
Tr04_c3_2d_512	20	2D central ignition, gridsize=512^2, $\rho_{c,9}$ = 2.9
Tr04_c3_3d_256	20	3D central ignition, gridsize=256^3, $\rho_{c,9}$ = 2.9
Tr04_c3_3d_256_9Tp†	20	3D central ignition, gridsize=256^3, $\rho_{c,9}$ = 2.9
Tr04_b5_3d_256	20	3D multi-point ignition, 5 bubbles, gridsize=256^3, $\rho_{c,9}$ = 2.9
Tr04_b30_3d_768	20	3D multi-point ignition, 30 bubbles, gridsize=768^3, $\rho_{c,9}$ = 2.9

Notes. The central density of the white dwarf ($\rho_{c,7}$ and $\rho_{c,9}$) is given in units of 10^7 and $10^9 \rm gcm^{-3}$, respectively. The density of the deflagration-to-detonation transition ($\rho_{T,7}$) is given in units of $10^7 \rm gcm^{-3}$. The mass fraction of the carbon/oxygen ratio (C/O) of the WD and The ^{12}C +^{16} O reaction rate ($f_{^{12}C+^{16}O}$) are dimensionless. The initial mass of the WD ($M_{\rm WD}$), CO core ($M_{\rm CO}$), He envelope ($M_{\rm He}$) are in units of $M_\odot$. The initial mass fraction composition of WD (C/O/Ne) are given by mass fraction of ^{12}C/^{16}O/^{22}Ne. The SNIa models assume different solar values in the initial composition ($Z_{\rm init}$) (for details, see references). †The authors allowed the nucleosynthesis calculations only starting at 90% of the temperature peak ($\sim$ 8.5 x 10^9 K) for those tracer particles that reach NSE conditions.

References. (1) Fink et al. (2014); (2) Iwamoto et al. (1999); (3) Kromer et al. (2013); (4) Kromer et al. (2015); (5) Kromer et al. (2016); (6) Leung & Nomoto (2018); (7) Leung & Nomoto (2020a); (8) Leung & Nomoto (2020b); (9) Maeda et al. (2010); (10) Marquardt et al. (2015); (11) Ohlmann et al. (2014); (12) Pakmor et al. (2010); (13) Pakmor et al. (2012); (14) Papish & Perets (2016) (15) Seitenzahl et al. (2013); (16) Seitenzahl et al. (2016); (17) Shen et al. (2018); (18) Sim et al. (2010); (19) Sim et al. (2012); (20) Travaglio et al. (2004).

Table 2. List of SNcc explosion models in this study.

Model Name	Ref.	Basic Proprieties
Ch04_SNII_Z0	a	Type II Supernova, $Z_{\rm init}$ = 0, $(m_{\rm low}, m_{\rm up}) = (13, 35)\rm M_\odot$
Ch04_SNII_Z_1E-6	a	Type II Supernova, $Z_{\rm init}$ = 1E-06, $(m_{\rm low}, m_{\rm up}) = (13, 35)\rm M_\odot$
Ch04_SNII_Z_1E-4	a	Type II Supernova, $Z_{\rm init}$ = 1E-04, $(m_{\rm low}, m_{\rm up}) = (13, 35)\rm M_\odot$
Ch04_SNII_Z_1E-3	a	Type II Supernova, $Z_{\rm init}$ = 1E-03, $(m_{\rm low}, m_{\rm up}) = (13, 35)\rm M_\odot$
Ch04_SNII_Z_6E-3	a	Type II Supernova, $Z_{\rm init}$ = 6E-03, $(m_{\rm low}, m_{\rm up}) = (13, 35)\rm M_\odot$
Ch04_SNII_Z_2E-2	a	Type II Supernova, $Z_{\rm init}$ = 2E-02, $(m_{\rm low}, m_{\rm up}) = (13, 35)\rm M_\odot$
No97_SNII_Z0	b	Type II Supernova, $Z_{\rm init}$ = 0, $(m_{\rm low}, m_{\rm up}) = (11, 50)\rm M_\odot$
No06_SNII_Z004	c	Type II Supernova, $Z_{\rm init}$ = 0.004, $(m_{\rm low}, m_{\rm up}) = (13, 40)\rm M_\odot$
No06_SNII_Z02	c	Type II Supernova, $Z_{\rm init}$ = 0.02, $(m_{\rm low}, m_{\rm up}) = (13, 40)\rm M_\odot$
No06_HN_Z02	c	Hypernovae, $Z_{\rm init}$ = 0.02, $(m_{\rm low}, m_{\rm up}) = (20, 40)\rm M_\odot$
No13_SNII_Z0	c,d	Type II Supernova, $Z_{\rm init}$ = 0, $(m_{\rm low}, m_{\rm up}) = (11, 40)\rm M_\odot$
No13_SNII_Z0_ext	c,d	Type II Supernova, $Z_{\rm init}$ = 0, $(m_{\rm low}, m_{\rm up}) = (11, 140)\rm M_\odot$
No13_SNII_Z001	c,d	Type II Supernova, $Z_{\rm init}$ = 0.001, $(m_{\rm low}, m_{\rm up}) = (13, 40)\rm M_\odot$
No13_SNII_Z004	c,d,e	Type II Supernova, $Z_{\rm init}$ = 0.004, $(m_{\rm low}, m_{\rm up}) = (13, 40)\rm M_\odot$
No13_SNII_Z008	c,d	Type II Supernova, $Z_{\rm init}$ = 0.008, $(m_{\rm low}, m_{\rm up}) = (13, 40)\rm M_\odot$
No13_SNII_Z02	c,d,e	Type II Supernova, $Z_{\rm init}$ = 0.02, $(m_{\rm low}, m_{\rm up}) = (13, 40)\rm M_\odot$
No13_SNII_Z05	c,d	Type II Supernova, $Z_{\rm init}$ = 0.05, $[(m_{\rm low}, m_{\rm up}) = (13, 40)\rm M_\odot$
No13_HN_Z0	c,d	Hypernovae, $Z_{\rm init}$ = 0, $(m_{\rm low}, m_{\rm up}) = (20, 40)\rm M_\odot$
No13_HN_Z0_ext	c,d	Hypernovae, $Z_{\rm init}$ = 0, $(m_{\rm low}, m_{\rm up}) = (20, 140)\rm M_\odot$
No13_HN_Z001	c,d	Hypernovae, $Z_{\rm init}$ = 0.001, $(m_{\rm low}, m_{\rm up}) = (20, 40)\rm M_\odot$
No13_HN_Z004	c,d	Hypernovae, $Z_{\rm init}$ = 0.004, $(m_{\rm low}, m_{\rm up}) = (20, 40)\rm M_\odot$
No13_HN_Z008	c,d	Hypernovae, $Z_{\rm init}$ = 0.008, $(m_{\rm low}, m_{\rm up}) = (20, 40)\rm M_\odot$
No13_HN_Z02	c,d,e	Hypernovae, $Z_{\rm init}$ = 0.02, $(m_{\rm low}, m_{\rm up}) = (20, 40)\rm M_\odot$
No13_HN_Z05	c,d	Hypernovae, $Z_{\rm init}$ = 0.05, $(m_{\rm low}, m_{\rm up}) = (20, 40)\rm M_\odot$
No13_PISN_Z0	c,d	Pair-instability, $Z_{\rm init}$ = 0, $(m_{\rm low}, m_{\rm up}) = (140, 300)\rm M_\odot$
No13_SNII+PISN_Z0	c,d	Type II Supernova and Pair-instability, $Z_{\rm init}$ = 0, $(m_{\rm low}, m_{\rm up}) = (11, 300)\rm M_\odot$
He10_SNII_Z0	f,g	Type II Supernova, $Z_{\rm init}$ = 0, $(m_{\rm low}, m_{\rm up}) = (10, 100)\rm M_\odot$
He02_PISN_Z0	f,g	Type II Supernova, $Z_{\rm init}$ = 0, $(m_{\rm low}, m_{\rm up}) = (140, 260)\rm M_\odot$
He0210_SNII+PISN_Z0	f,g	Type II SN and Pair-instability, $Z_{\rm init}$ = 0, $(m_{\rm low}, m_{\rm up}) = (10, 260)\rm M_\odot$
Su16_N20	h	Nonrotating SN1987A model calibrated by Nomoto & Hashimoto (1988), $Z_{\rm init}$ = 1, $(m_{\rm low}, m_{\rm up}) = (12.25, 120)\rm M_\odot$
Su16_W18	h	Rotating SN1987A model calibrated by Utrobin et al. (2015), $Z_{\rm init}$ = 1, $(m_{\rm low}, m_{\rm up}) = (12.25, 120)\rm M_\odot$

Notes. m, $m_{\rm low}$ and $m_{\rm up}$ are the initial, lowest, and greatest progenitor stellar mass simulated (in units of $\rm M_\odot$) for a given SNcc model which has an initial metallicity $Z_{\rm init}$ (in units of $Z_\odot$). The SNcc models can assume different solar values to define their initial metallicity composition ($Z_{\rm init}$) (for details, see references).

References. (a) Chieffi & Limongi (2004); (b) Nomoto et al. (1997); (c) Nomoto et al. (2006); (d) Nomoto et al. (2013); (e) Kobayashi et al. (2011); (f) Heger & Woosley (2002); (g) Heger & Woosley (2010); (h) Sukhbold et al. (2016).

Table 3. Numerical elemental abundances for projected spatial inner regions, as described in Section **??**. Chemical abundances of the elements of interest O, Ne, Mg, Si, S, Ar, Ca, Fe and Ni, are normalized by the abundance in the solar value (in our case ANGR, regard to the numerical abundance of the H. The indicated errors are 68% confidence limits.

		Elemental Abundances ($Z_\odot$)								
Name	T(keV)	Ar	Ca	Fe	Mg	Ne	Ni	O	S	Si
NGC 5846 Group	$0.750^{+0.003}_{0.003}$	$2.62^{+0.46}_{-0.46}$	$2.52^{+0.90}_{-0.90}$	$0.444^{+0.011}_{-0.011}$	$0.752^{+0.034}_{-0.034}$	$1.16^{+0.07}_{-0.07}$	$0.325^{+0.094}_{-0.094}$	$0.342^{+0.058}_{-0.058}$	$0.917^{+0.081}_{-0.081}$	$0.957^{+0.038}_{-0.038}$
NGC 4472 Group	$0.873^{+0.005}_{-0.005}$	$0.65^{+0.38}_{-0.38}$	$0.29^{+0.19}_{-0.19}$	$0.421^{+0.020}_{-0.020}$	$0.811^{+0.049}_{-0.049}$	$1.28^{+0.11}_{-0.11}$	$1.59^{+0.20}_{-0.20}$	$0.35^{+0.06}_{-0.06}$	$0.846^{+0.093}_{-0.093}$	$0.861^{+0.048}_{-0.048}$
HCG62	$0.893^{+0.005}_{-0.005}$	$0.51^{+0.26}_{-0.26}$	$0.37^{+0.23}_{-0.23}$	$0.318^{+0.014}_{-0.014}$	$0.596^{+0.044}_{-0.044}$	$0.60^{+0.10}_{-0.10}$	$2.02^{+0.19}_{-0.19}$	$0.065^{+0.031}_{-0.031}$	$0.802^{+0.075}_{-0.075}$	$0.719^{+0.037}_{-0.037}$
Ophiuchus Cluster	$7.09^{+0.08}_{-0.08}$	$1.43^{+0.30}_{-0.30}$	$0.72^{+0.28}_{-0.28}$	$0.458^{+0.014}_{-0.014}$	$0.71^{+0.20}_{-0.20}$	$1.35^{+0.32}_{-0.32}$	$0.62^{+0.22}_{-0.22}$	$0.31^{+0.20}_{-0.20}$	$1.09^{+0.13}_{-0.13}$	$0.94^{+0.11}_{-0.11}$
NGC 1550 Group	$1.272^{+0.004}_{-0.004}$	$0.78^{+0.15}_{-0.15}$	$1.04^{+0.26}_{-0.26}$	$0.355^{+0.012}_{-0.012}$	$0.48^{+0.05}_{-0.05}$	$0.41^{+0.12}_{-0.12}$	$0.73^{+0.10}_{-0.10}$	$0.168^{+0.064}_{-0.064}$	$0.558^{+0.044}_{-0.044}$	$0.55^{+0.03}_{-0.03}$
Abell 3581	$1.573^{+0.009}_{-0.009}$	$0.893^{+0.098}_{-0.098}$	$0.85^{+0.15}_{-0.15}$	$0.418^{+0.011}_{-0.011}$	$0.568^{+0.035}_{-0.035}$	$0.537^{+0.093}_{-0.093}$	$1.01^{+0.08}_{-0.08}$	$0.644^{+0.054}_{-0.054}$	$0.59^{+0.03}_{-0.03}$	$0.716^{+0.023}_{-0.023}$
NGC 507 Group	$1.213^{+0.007}_{-0.007}$	$0.84^{+0.15}_{-0.15}$	$1.43^{+0.29}_{-0.29}$	$0.325^{+0.016}_{-0.016}$	$0.57^{+0.04}_{-0.04}$	$0.340^{+0.097}_{-0.097}$	$1.74^{+0.13}_{-0.13}$	$0.21^{+0.07}_{-0.07}$	$0.65^{+0.04}_{-0.04}$	$0.75^{+0.02}_{-0.02}$
Perseus Cluster	$3.835^{+0.005}_{-0.005}$	$0.882^{+0.037}_{-0.037}$	$0.759^{+0.036}_{-0.036}$	$0.5042^{+0.0024}_{-0.0024}$	$0.787^{+0.022}_{-0.022}$	$1.331^{+0.029}_{-0.029}$	$0.84^{+0.04}_{-0.04}$	$0.474^{+0.029}_{-0.029}$	$0.684^{+0.015}_{-0.015}$	$0.778^{+0.012}_{-0.012}$
Abell 496	$3.17^{+0.02}_{-0.02}$	$0.89^{+0.13}_{-0.13}$	$0.79^{+0.13}_{-0.13}$	$0.521^{+0.009}_{-0.009}$	$0.933^{+0.077}_{-0.077}$	$1.58^{+0.11}_{-0.11}$	$0.74^{+0.14}_{-0.14}$	$0.44^{+0.1}_{-0.1}$	$0.795^{+0.053}_{-0.053}$	$0.921^{+0.043}_{-0.043}$
Abell 3571	$6.53^{+0.05}_{-0.05}$	$0.93^{+0.35}_{-0.35}$	$0.52^{+0.22}_{-0.22}$	$0.347^{+0.013}_{-0.013}$	$0.47^{+0.21}_{-0.21}$	$0.088^{+0.064}_{-0.064}$	$0.42^{+0.17}_{-0.17}$	$0.30^{+0.19}_{-0.19}$	$0.50^{+0.15}_{-0.15}$	$0.36^{+0.12}_{-0.12}$
Abell 262	$1.658^{+0.007}_{-0.007}$	$0.88^{+0.15}_{-0.15}$	$0.95^{+0.22}_{-0.22}$	$0.426^{+0.011}_{-0.011}$	$0.599^{+0.059}_{-0.059}$	$0.52^{+0.11}_{-0.11}$	$0.87^{+0.13}_{-0.13}$	$0.069^{+0.041}_{-0.041}$	$0.768^{+0.048}_{-0.048}$	$0.742^{+0.036}_{-0.036}$
NGC 2300 Group	$0.776^{+0.013}_{-0.013}$	$0.80^{+0.47}_{-0.47}$	$0.80^{+0.16}_{-0.16}$	$0.204^{+0.023}_{-0.023}$	$0.456^{+0.086}_{-0.086}$	$0.74^{+0.16}_{-0.16}$	$0.23^{+0.14}_{-0.14}$	$0.21^{+0.12}_{-0.12}$	$0.90^{+0.21}_{-0.21}$	$0.598^{+0.084}_{-0.084}$
Centaurus Cluster	$1.820^{+0.002}_{-0.002}$	$1.113^{+0.069}_{-0.069}$	$1.37^{+0.09}_{-0.09}$	$0.782^{+0.005}_{-0.005}$	$0.756^{+0.033}_{-0.033}$	$1.54^{+0.06}_{-0.06}$	$1.618^{+0.061}_{-0.061}$	$0.011^{+0.007}_{-0.007}$	$1.156^{+0.026}_{-0.026}$	$1.232^{+0.019}_{-0.019}$
MKW4 Cluster	$1.66^{+0.02}_{-0.02}$	$1.64^{+0.47}_{-0.47}$	$1.14^{+0.63}_{-0.63}$	$0.860^{+0.076}_{-0.076}$	$0.70^{+0.19}_{-0.19}$	$1.52^{+0.57}_{-0.57}$	$1.88^{+0.48}_{-0.48}$	$0.70^{+0.22}_{-0.22}$	$1.29^{+0.16}_{-0.16}$	$1.63^{+0.15}_{-0.15}$
NGC 5044 Group	$0.878^{+0.004}_{-0.004}$	$0.65^{+0.19}_{-0.19}$	$0.41^{+0.21}_{-0.21}$	$0.324^{+0.012}_{-0.012}$	$0.746^{+0.032}_{-0.032}$	$0.82^{+0.08}_{-0.08}$	$2.47^{+0.13}_{-0.13}$	$0.203^{+0.037}_{-0.037}$	$0.75^{+0.05}_{-0.05}$	$0.629^{+0.026}_{-0.026}$
AWM7 Cluster	$3.03^{+0.06}_{-0.06}$	$1.29^{+0.31}_{-0.31}$	$1.52^{+0.34}_{-0.34}$	$0.850^{+0.037}_{-0.037}$	$1.37^{+0.19}_{-0.19}$	$1.16^{+0.27}_{-0.27}$	$2.25^{+0.34}_{-0.34}$	$0.27^{+0.14}_{-0.14}$	$0.98^{+0.13}_{-0.13}$	$1.50^{+0.11}_{-0.11}$
NGC 6338 Group	$1.868^{+0.036}_{-0.036}$	$0.39^{+0.25}_{-0.25}$	$0.38^{+0.24}_{-0.24}$	$0.552^{+0.067}_{-0.067}$	$0.29^{+0.16}_{-0.16}$	$1.85^{+0.74}_{-0.74}$	$0.36^{+0.22}_{-0.22}$	$0.31^{+0.20}_{-0.20}$	$1.18^{+0.25}_{-0.25}$	$0.91^{+0.18}_{-0.18}$
UGC03957 Group	$2.50^{+0.04}_{-0.04}$	$1.59^{+0.34}_{-0.34}$	$1.19^{+0.34}_{-0.34}$	$0.628^{+0.026}_{-0.026}$	$1.28^{+0.17}_{-0.17}$	$0.73^{+0.21}_{-0.21}$	$1.40^{+0.35}_{-0.35}$	$0.45^{+0.17}_{-0.17}$	$0.94^{+0.14}_{-0.14}$	$1.06^{+0.11}_{-0.11}$

Table 4. Same as Table 3, but for outer regions.

		Elemental Abundances ($Z_\odot$)								
Name	T(keV)	Ar	Ca	Fe	Mg	Ne	Ni	O	S	Si
NGC 5846 Group	$0.949706^{+0.01}_{-0.01}$	$0.25^{+0.18}_{-0.18}$	$0.29^{+0.24}_{-0.24}$	$0.134^{+0.018}_{-0.018}$	$0.149^{+0.079}_{-0.079}$	$0.50^{+0.16}_{-0.16}$	$1.42^{+0.26}_{-0.26}$	$0.20^{+0.15}_{-0.15}$	$0.73^{+0.16}_{-0.16}$	$0.444^{+0.068}_{-0.068}$
NGC 4472 Group	$1.296140^{+0.006}_{-0.006}$	$1.37^{+0.27}_{-0.27}$	$0.47^{+0.23}_{-0.23}$	$0.34^{+0.02}_{-0.02}$	$0.795^{+0.064}_{-0.064}$	$0.74^{+0.14}_{-0.14}$	$1.71^{+0.16}_{-0.16}$	$0.25^{+0.14}_{-0.14}$	$0.968^{+0.072}_{-0.072}$	$1.009^{+0.048}_{-0.048}$
HCG62	$1.123590^{+0.01}_{-0.01}$	$0.23^{+0.10}_{-0.10}$	$0.36^{+0.20}_{-0.20}$	$0.068^{+0.007}_{-0.007}$	$0.257^{+0.057}_{-0.057}$	$0.20^{+0.06}_{-0.06}$	$0.736^{+0.088}_{-0.088}$	$0.30^{+0.12}_{-0.12}$	$0.27^{+0.06}_{-0.06}$	$0.29^{+0.03}_{-0.03}$
Ophiuchus Cluster	$8.249609^{+0.03}_{-0.03}$	$1.84^{+0.14}_{-0.14}$	$1.49^{+0.13}_{-0.13}$	$0.210^{+0.004}_{-0.004}$	$1.53^{+0.09}_{-0.09}$	$0.25^{+0.14}_{-0.14}$	$0.25^{+0.14}_{-0.14}$	$0.127^{+0.082}_{-0.082}$	$0.626^{+0.059}_{-0.059}$	$0.486^{+0.047}_{-0.047}$
NGC 1550 Group	$1.344191^{+0.008}_{-0.008}$	$0.33^{+0.15}_{-0.15}$	$0.26^{+0.16}_{-0.16}$	$0.218^{+0.012}_{-0.012}$	$0.503^{+0.058}_{-0.058}$	$0.54^{+0.13}_{-0.13}$	$0.91^{+0.12}_{-0.12}$	$0.062^{+0.046}_{-0.046}$	$0.41^{+0.05}_{-0.05}$	$0.389^{+0.031}_{-0.031}$
Abell 3581	$1.649313^{+0.02}_{-0.02}$	$0.22^{+0.11}_{-0.11}$	$0.66^{+0.28}_{-0.28}$	$0.212^{+0.015}_{-0.015}$	$0.139^{+0.057}_{-0.057}$	$0.28^{+0.14}_{-0.14}$	$0.132^{+0.079}_{-0.079}$	$0.125^{+0.073}_{-0.073}$	$0.236^{+0.055}_{-0.055}$	$0.241^{+0.035}_{-0.035}$
NGC 507 Group	$1.326627^{+0.008}_{-0.008}$	$0.33^{+0.15}_{-0.15}$	$0.30^{+0.14}_{-0.14}$	$0.198^{+0.012}_{-0.012}$	$0.505^{+0.048}_{-0.048}$	$0.63^{+0.11}_{-0.11}$	$1.52^{+0.11}_{-0.11}$	$0.25^{+0.12}_{-0.12}$	$0.42^{+0.051}_{-0.051}$	$0.473^{+0.023}_{-0.023}$
Perseus Cluster	$5.130343^{+0.01}_{-0.01}$	$0.58^{+0.07}_{-0.07}$	$0.52^{+0.07}_{-0.07}$	$0.282^{+0.003}_{-0.003}$	$0.551^{+0.043}_{-0.043}$	$0.62^{+0.05}_{-0.05}$	$0.495^{+0.064}_{-0.064}$	$0.244^{+0.048}_{-0.048}$	$0.33^{+0.03}_{-0.03}$	$0.421^{+0.024}_{-0.024}$
Abell 496	$3.998466^{+0.03}_{-0.03}$	$0.85^{+0.23}_{-0.23}$	$0.49^{+0.22}_{-0.22}$	$0.234^{+0.011}_{-0.011}$	$0.99^{+0.13}_{-0.13}$	$0.85^{+0.17}_{-0.17}$	$1.26^{+0.23}_{-0.23}$	$0.015^{+0.014}_{-0.014}$	$0.345^{+0.082}_{-0.082}$	$0.467^{+0.072}_{-0.072}$
Abell 3571	$5.198524^{+0.05}_{-0.05}$	$1.11^{+0.36}_{-0.36}$	$0.08^{+0.06}_{-0.06}$	$0.186^{+0.013}_{-0.013}$	$0.73^{+0.21}_{-0.21}$	$0.047^{+0.032}_{-0.032}$	$0.38^{+0.21}_{-0.21}$	$0.78^{+0.26}_{-0.26}$	$0.31^{+0.14}_{-0.14}$	$0.39^{+0.12}_{-0.12}$
Abell 262	$2.130440^{+0.01}_{-0.01}$	$0.41^{+0.12}_{-0.12}$	$0.82^{+0.18}_{-0.18}$	$0.335^{+0.010}_{-0.010}$	$0.797^{+0.075}_{-0.075}$	$0.72^{+0.11}_{-0.11}$	$1.34^{+0.15}_{-0.15}$	$0.038^{+0.029}_{-0.029}$	$0.46^{+0.05}_{-0.05}$	$0.58^{+0.04}_{-0.04}$
NGC 2300 Group	$1.051555^{+0.06}_{-0.06}$	$1.20^{+1.10}_{-1.10}$	$2.54^{+0.57}_{-0.57}$	$0.110^{+0.073}_{-0.07}$	$0.42^{+0.30}_{-0.30}$	$1.98^{+0.90}_{-0.90}$	$1.08^{+0.90}_{-0.90}$	$0.25^{+0.18}_{-0.18}$	$2.50^{+1.20}_{-1.20}$	$0.41^{+0.30}_{-0.30}$
Centaurus Cluster	$3.349613^{+0.01}_{-0.01}$	$0.55^{+0.11}_{-0.11}$	$0.57^{+0.11}_{-0.11}$	$0.366^{+0.007}_{-0.007}$	$0.689^{+0.062}_{-0.062}$	$0.807^{+0.078}_{-0.078}$	$0.75^{+0.12}_{-0.12}$	$0.025^{+0.014}_{-0.014}$	$0.497^{+0.044}_{-0.044}$	$0.678^{+0.035}_{-0.035}$
MKW4 Cluster	$1.720358^{+0.02}_{-0.02}$	$1.25^{+0.37}_{-0.37}$	$0.41^{+0.20}_{-0.20}$	$0.256^{+0.023}_{-0.023}$	$0.45^{+0.15}_{-0.15}$	$0.30^{+0.15}_{-0.15}$	$1.13^{+0.28}_{-0.28}$	$0.136^{+0.087}_{-0.087}$	$0.47^{+0.11}_{-0.11}$	$0.572^{+0.087}_{-0.087}$
NGC 5044 Group	$1.220737^{+0.01}_{-0.01}$	$0.48^{+0.22}_{-0.22}$	$0.36^{+0.19}_{-0.19}$	$0.28^{+0.02}_{-0.02}$	$0.529^{+0.054}_{-0.054}$	$0.80^{+0.14}_{-0.14}$	$1.05^{+0.16}_{-0.16}$	$0.206^{+0.072}_{-0.072}$	$0.474^{+0.058}_{-0.058}$	$0.425^{+0.033}_{-0.033}$
AWM7 Cluster	$3.438994^{+0.02}_{-0.02}$	$0.74^{+0.16}_{-0.16}$	$0.50^{+0.13}_{-0.13}$	$0.318^{+0.009}_{-0.009}$	$0.870^{+0.098}_{-0.098}$	$0.43^{+0.10}_{-0.10}$	$1.51^{+0.19}_{-0.19}$	$0.025^{+0.017}_{-0.017}$	$0.411^{+0.065}_{-0.065}$	$0.561^{+0.051}_{-0.051}$
NGC 6338 Group	$1.669503^{+0.07}_{-0.07}$	$0.35^{+0.23}_{-0.23}$	$0.34^{+0.21}_{-0.21}$	$0.027^{+0.018}_{-0.018}$	$0.32^{+0.17}_{-0.17}$	$0.38^{+0.23}_{-0.23}$	$0.58^{+0.21}_{-0.21}$	$0.27^{+0.17}_{-0.17}$	$0.53^{+0.15}_{-0.15}$	$0.511^{+0.095}_{-0.095}$
UGC03957 Group	$2.295106^{+0.075}_{-0.0075}$	$0.26^{+0.14}_{-0.14}$	$1.26^{+0.63}_{-0.63}$	$0.345^{+0.061}_{-0.061}$	$1.36^{+0.37}_{-0.37}$	$0.47^{+0.21}_{-0.21}$	$3.03^{+0.78}_{-0.78}$	$0.23^{+0.12}_{-0.12}$	$1.14^{+0.26}_{-0.26}$	$1.04^{+0.21}_{-0.21}$

Table 5. Same as Table 3, but for outer regions.

		Elemental Abundances ($Z_{\odot}$)								
Name	T(keV)	Ar	Ca	Fe	Mg	Ne	Ni	O	S	Si
NGC 5846 Group	$0.773^{+0.003}_{-0.003}$	$0.45^{+0.30}_{-0.30}$	$0.25^{+0.18}_{-0.18}$	$0.242^{+0.007}_{-0.007}$	$0.475^{+0.020}_{-0.020}$	$0.792^{+0.043}_{-0.043}$	$1.171^{+0.096}_{-0.096}$	$0.038^{+0.027}_{-0.027}$	$0.851^{+0.054}_{-0.054}$	$0.664^{+0.020}_{-0.020}$
NGC 4472 Group	$1.107^{+0.002}_{-0.002}$	$0.999^{+0.090}_{-0.090}$	$0.034^{+0.018}_{-0.018}$	$0.325^{+0.004}_{-0.004}$	$0.431^{+0.015}_{-0.015}$	$0.218^{+0.035}_{-0.035}$	$0.484^{+0.033}_{-0.033}$	$0.024^{+0.021}_{-0.021}$	$0.74^{+0.02}_{-0.02}$	$0.664^{+0.011}_{-0.011}$
HCG62	$0.996^{+0.002}_{-0.002}$	$0.489^{+0.088}_{-0.088}$	$0.53^{+0.18}_{-0.18}$	$0.1393^{+0.0025}_{-0.0025}$	$0.282^{+0.014}_{-0.014}$	$0.29^{+0.03}_{-0.03}$	$0.974^{+0.034}_{-0.034}$	$0.009^{+0.006}_{-0.006}$	$0.458^{+0.022}_{-0.022}$	$0.411^{+0.010}_{-0.010}$
Ophiuchus Cluster	$8.62^{+0.02}_{-0.02}$	$1.258^{+0.085}_{-0.085}$	$0.783^{+0.081}_{-0.081}$	$0.317^{+0.003}_{-0.003}$	$0.824^{+0.057}_{-0.057}$	$0.34^{+0.078}_{-0.08}$	$0.053^{+0.034}_{-0.034}$	$1.62^{+0.14}_{-0.14}$	$0.514^{+0.036}_{-0.036}$	$0.31^{+0.03}_{-0.03}$
NGC 1550 Group	$1.322^{+0.002}_{-0.002}$	$0.499^{+0.054}_{-0.054}$	$0.61^{+0.10}_{-0.10}$	$0.221^{+0.004}_{-0.004}$	$0.42^{+0.02}_{-0.02}$	$0.485^{+0.037}_{-0.037}$	$0.90^{+0.04}_{-0.04}$	$0.175^{+0.035}_{-0.035}$	$0.44^{+0.02}_{-0.02}$	$0.455^{+0.001}_{-0.01}$
Abell 3581	$1.657^{+0.003}_{-0.003}$	$0.68^{+0.057}_{-0.057}$	$0.809^{+0.088}_{-0.088}$	$0.3307^{+0.0043}_{-0.0043}$	$0.350^{+0.025}_{-0.025}$	$0.56^{+0.05}_{-0.05}$	$0.501^{+0.044}_{-0.044}$	$0.497^{+0.035}_{-0.035}$	$0.45^{+0.02}_{-0.02}$	$0.493^{+0.013}_{-0.013}$
NGC 507 Group	$1.275^{+0.003}_{-0.003}$	$0.634^{+0.077}_{-0.077}$	$1.00^{+0.14}_{-0.14}$	$0.235^{+0.005}_{-0.005}$	$0.47^{+0.02}_{-0.02}$	$0.539^{+0.047}_{-0.047}$	$1.378^{+0.053}_{-0.053}$	$0.25^{+0.12}_{-0.12}$	$0.50^{+0.02}_{-0.02}$	$0.585^{+0.012}_{-0.012}$
Perseus Cluster	$4.297^{+0.004}_{-0.004}$	$0.476^{+0.027}_{-0.027}$	$0.463^{+0.026}_{-0.026}$	$0.4035^{+0.0014}_{-0.0014}$	$0.559^{+0.016}_{-0.016}$	$1.35^{+0.02}_{-0.02}$	$0.721^{+0.028}_{-0.028}$	$0.912^{+0.022}_{-0.022}$	$0.391^{+0.011}_{-0.011}$	$0.543^{+0.009}_{-0.009}$
Abell 496	$3.76^{+0.01}_{-0.01}$	$0.767^{+0.087}_{-0.087}$	$0.754^{+0.088}_{-0.088}$	$0.381^{+0.005}_{-0.005}$	$0.753^{+0.052}_{-0.052}$	$1.261^{+0.071}_{-0.071}$	$0.725^{+0.098}_{-0.098}$	$0.161^{+0.058}_{-0.058}$	$0.572^{+0.036}_{-0.036}$	$0.632^{+0.029}_{-0.029}$
Abell 3571	$6.22^{+0.03}_{-0.03}$	$0.78^{+0.19}_{-0.19}$	$0.67^{+0.18}_{-0.18}$	$0.3007^{+0.0065}_{-0.0065}$	$0.167^{+0.084}_{-0.084}$	$0.25^{+0.14}_{-0.14}$	$0.22^{+0.13}_{-0.13}$	$0.92^{+0.14}_{-0.14}$	$0.457^{+0.076}_{-0.076}$	$0.292^{+0.060}_{-0.060}$
Abell 262	$2.057^{+0.007}_{-0.007}$	$0.558^{+0.067}_{-0.067}$	$0.788^{+0.088}_{-0.088}$	$0.3597^{+0.0065}_{-0.0065}$	$0.558^{+0.035}_{-0.035}$	$0.942^{+0.063}_{-0.063}$	$0.609^{+0.069}_{-0.069}$	$0.048^{+0.029}_{-0.029}$	$0.514^{+0.025}_{-0.025}$	$0.575^{+0.018}_{-0.018}$
NGC 2300 Group	$0.94^{+0.02}_{-0.02}$	$1.02^{+0.60}_{-0.60}$	$0.29^{+0.24}_{-0.24}$	$0.146^{+0.015}_{-0.015}$	$0.24^{+0.07}_{-0.07}$	$0.58^{+0.17}_{-0.17}$	$0.128^{+0.097}_{-0.097}$	$0.26^{+0.17}_{-0.17}$	$0.55^{+0.12}_{-0.12}$	$0.404^{+0.071}_{-0.071}$
Centaurus Cluster	$2.814^{+0.006}_{-0.006}$	$0.728^{+0.047}_{-0.047}$	$0.97^{+0.05}_{-0.05}$	$0.668^{+0.004}_{-0.004}$	$0.568^{+0.027}_{-0.027}$	$2.444^{+0.042}_{-0.042}$	$0.686^{+0.054}_{-0.054}$	$0.097^{+0.036}_{-0.036}$	$0.754^{+0.019}_{-0.019}$	$0.900^{+0.015}_{-0.015}$
MKW4 Cluster	$1.722^{+0.008}_{-0.008}$	$0.95^{+0.13}_{-0.13}$	$1.13^{+0.21}_{-0.21}$	$0.426^{+0.010}_{-0.010}$	$0.65^{+0.06}_{-0.06}$	$0.75^{+0.12}_{-0.12}$	$1.26^{+0.11}_{-0.11}$	$0.111^{+0.063}_{-0.063}$	$0.612^{+0.044}_{-0.044}$	$0.837^{+0.033}_{-0.033}$
NGC 5044 Group	$0.987^{+0.002}_{-0.002}$	$0.528^{+0.095}_{-0.095}$	$0.212^{+0.079}_{-0.079}$	$0.254^{+0.005}_{-0.005}$	$0.575^{+0.018}_{-0.018}$	$0.673^{+0.044}_{-0.044}$	$1.749^{+0.061}_{-0.061}$	$0.124^{+0.018}_{-0.018}$	$0.546^{+0.023}_{-0.023}$	$0.502^{+0.012}_{-0.012}$
AWM7 Cluster	$3.45^{+0.01}_{-0.01}$	$0.421^{+0.094}_{-0.094}$	$0.673^{+0.091}_{-0.091}$	$0.435^{+0.006}_{-0.006}$	$0.742^{+0.056}_{-0.056}$	$0.828^{+0.075}_{-0.075}$	$1.02^{+0.10}_{-0.10}$	$0.087^{+0.036}_{-0.036}$	$0.535^{+0.039}_{-0.039}$	$0.663^{+0.031}_{-0.031}$
NGC 6338 Group	$1.997^{+0.025}_{-0.025}$	$0.72^{+0.21}_{-0.21}$	$1.26^{+0.28}_{-0.28}$	$0.319^{+0.016}_{-0.016}$	$0.112^{+0.062}_{-0.062}$	$1.00^{+0.20}_{-0.20}$	$0.25^{+0.11}_{-0.11}$	$0.25^{+0.14}_{-0.14}$	$0.476^{+0.071}_{-0.071}$	$0.493^{+0.054}_{-0.054}$
UGC03957 Group	$2.54^{+0.02}_{-0.02}$	$1.10^{+0.21}_{-0.21}$	$0.81^{+0.22}_{-0.22}$	$0.494^{+0.018}_{-0.018}$	$0.96^{+0.12}_{-0.12}$	$1.00^{+0.17}_{-0.17}$	$1.64^{+0.22}_{-0.22}$	$0.28^{+0.14}_{-0.14}$	$0.745^{+0.081}_{-0.081}$	$0.861^{+0.057}_{-0.057}$

1 KS TEST EVALUATION IN THIS WORK FOR EACH INDICATOR.

2 REJECTION TIME OF KS TEST

REFERENCES

Chieffi A., Limongi M., 2004, ApJ, 608, 405
Fink M., et al., 2014, MNRAS, 438, 1762
Heger A., Woosley S. E., 2002, ApJ, 567, 532
Heger A., Woosley S. E., 2010, ApJ, 724, 341
Iwamoto K., Brachwitz F., Nomoto K., Kishimoto N., Umeda H., Hix W. R., Thielemann F.-K., 1999, ApJS, 125, 439
Kobayashi C., Karakas A. I., Umeda H., 2011, MNRAS, 414, 3231
Kromer M., et al., 2013, ApJ, 778, L18
Kromer M., et al., 2015, MNRAS, 450, 3045
Kromer M., et al., 2016, MNRAS, 459, 4428
Leung S.-C., Nomoto K., 2018, ApJ, 861, 143
Leung S.-C., Nomoto K., 2020a, ApJ, 888, 80
Leung S.-C., Nomoto K., 2020b, ApJ, 900, 54
Maeda K., Röpke F. K., Fink M., Hillebrandt W., Travaglio C., Thielemann F. K., 2010, ApJ, 712, 624
Marquardt K. S., Sim S. A., Ruiter A. J., Seitenzahl I. R., Ohlmann S. T., Kromer M., Pakmor R., Röpke F. K., 2015, A&A, 580, A118
Nomoto K., Hashimoto M., 1988, Phys. Rep., 163, 13
Nomoto K., Iwamoto K., Nakasato N., Thielemann F. K., Brachwitz F., Tsujimoto T., Kubo Y., Kishimoto N., 1997, Nuclear Phys. A, 621, 467
Nomoto K., Tominaga N., Umeda H., Kobayashi C., Maeda K., 2006, Nuclear Phys. A, 777, 424
Nomoto K., Kobayashi C., Tominaga N., 2013, ARA&A, 51, 457
Ohlmann S. T., Kromer M., Fink M., Pakmor R., Seitenzahl I. R., Sim S. A., Röpke F. K., 2014, A&A, 572, A57
Pakmor R., Kromer M., Röpke F. K., Sim S. A., Ruiter A. J., Hillebrandt W., 2010, Nature, 463, 61
Pakmor R., Kromer M., Taubenberger S., Sim S. A., Röpke F. K., Hillebrandt W., 2012, ApJ, 747, L10
Papish O., Perets H. B., 2016, ApJ, 822, 19
Seitenzahl I. R., et al., 2013, MNRAS, 429, 1156
Seitenzahl I. R., et al., 2016, A&A, 592, A57
Shen K. J., Kasen D., Miles B. J., Townsley D. M., 2018, ApJ, 854, 52
Sim S. A., Röpke F. K., Hillebrandt W., Kromer M., Pakmor R., Fink M., Ruiter A. J., Seitenzahl I. R., 2010, ApJ, 714, L52
Sim S. A., Fink M., Kromer M., Röpke F. K., Ruiter A. J., Hillebrandt W., 2012, MNRAS, 420, 3003
Sukhbold T., Ertl T., Woosley S. E., Brown J. M., Janka H. T., 2016, ApJ, 821, 38
Travaglio C., Hillebrandt W., Reinecke M., Thielemann F. K., 2004, A&A, 425, 1029
Utrobin V. P., Wongwathanarat A., Janka H. T., Müller E., 2015, A&A, 581, A40

This paper has been typeset from a TEX/LATEX file prepared by the author.

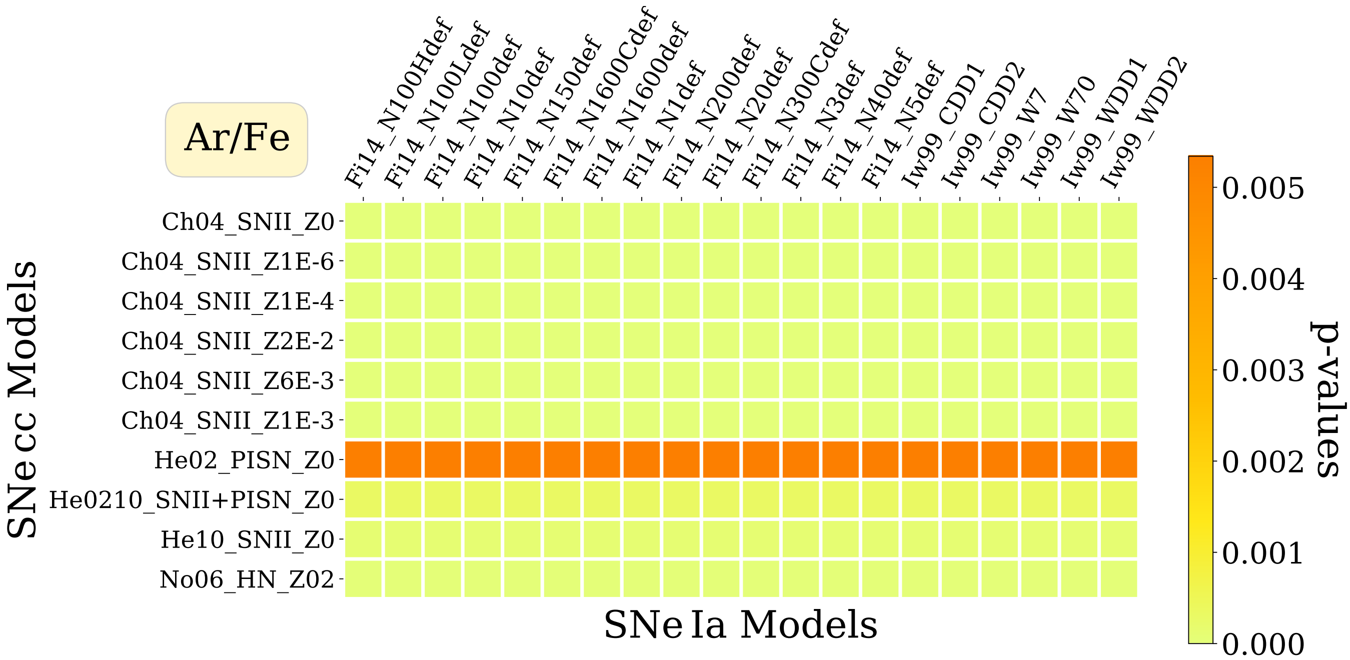

Figure 1. P-values of a few tested combinations of pair of SN model - SNIa+SNcc - using the Ar/Fe ratio at 2σ confidence level. Only a few of SN model combinations are represented for illustration. Results of p-values from KS test are described in Section 4.1.2. The color intensity represent the values in the colorbar, where more orange cells have greater p-values.

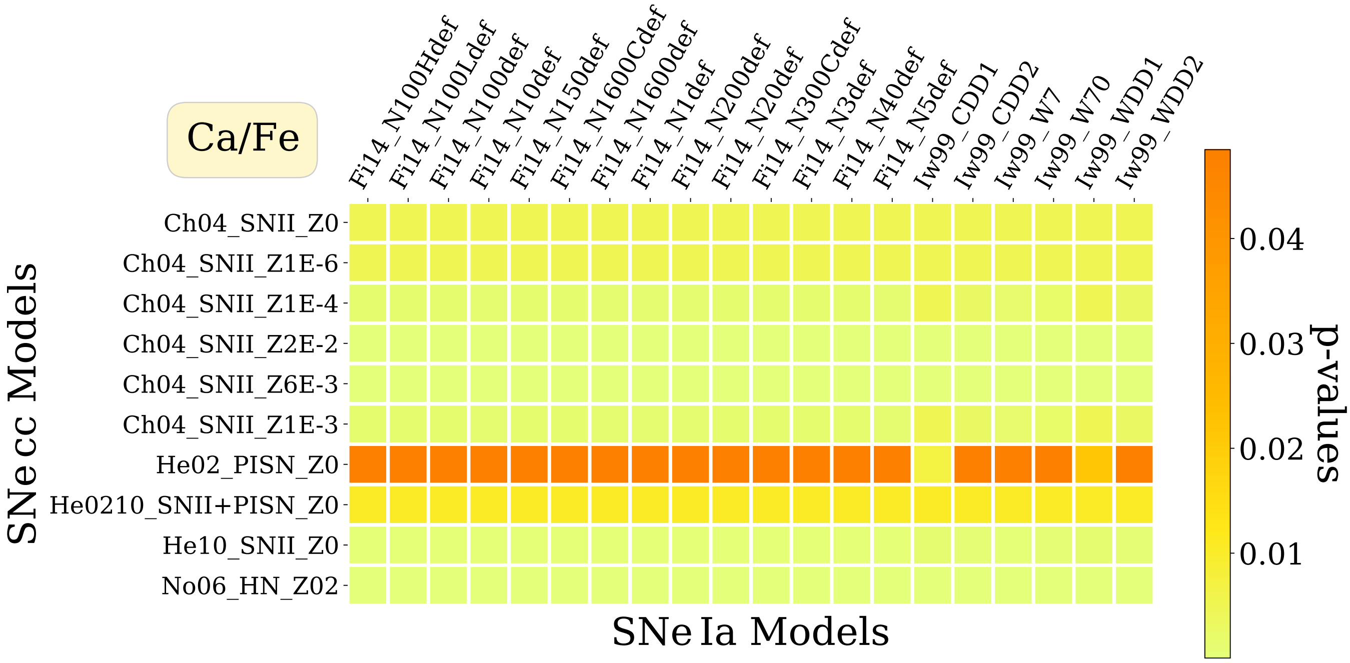

Figure 2. Same as Figure 1 but for Ca/Fe ratio.

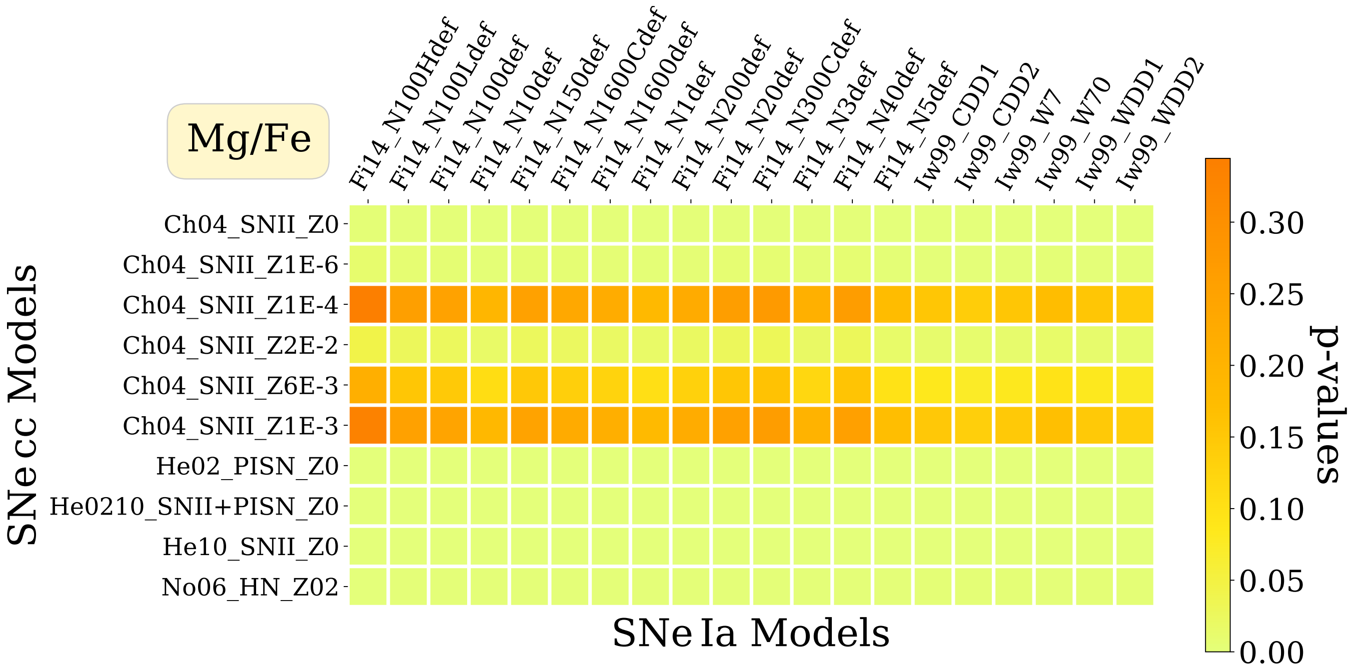

Figure 3. Same as Figure 1 but for Mg/Fe ratio.

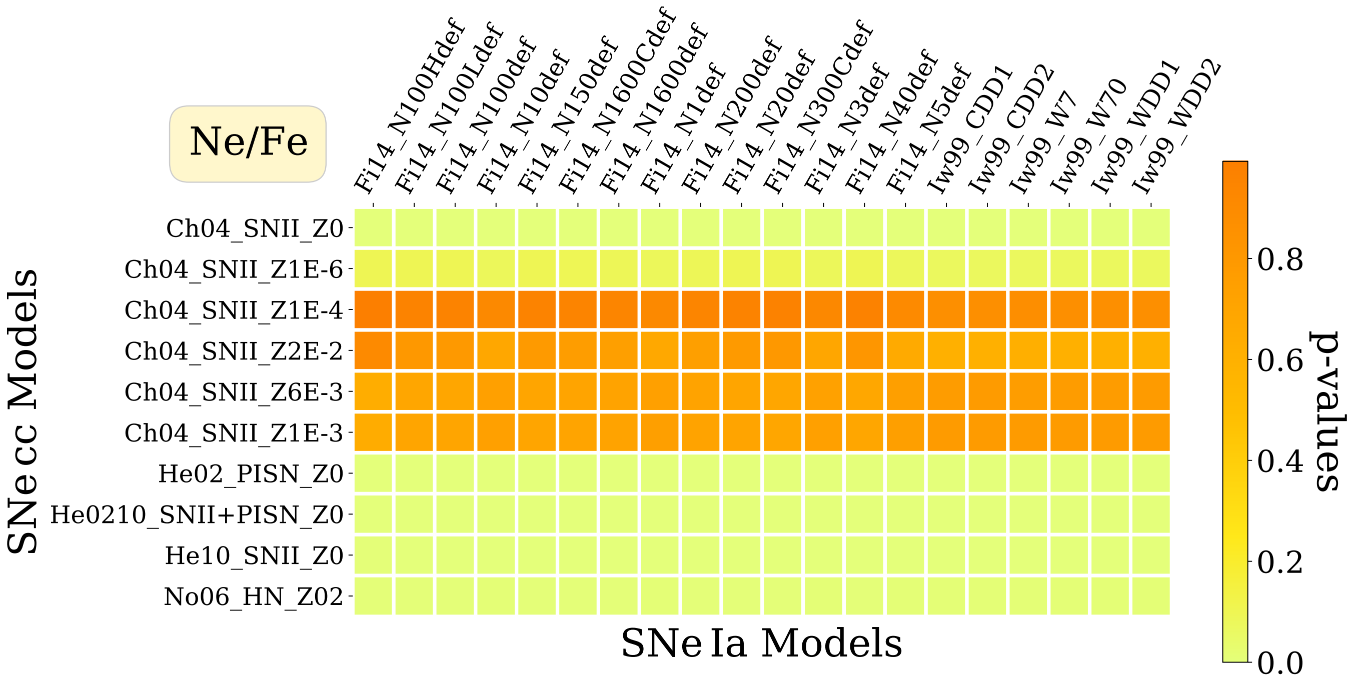

Figure 4. Same as Figure 1 but for Ne/Fe ratio.

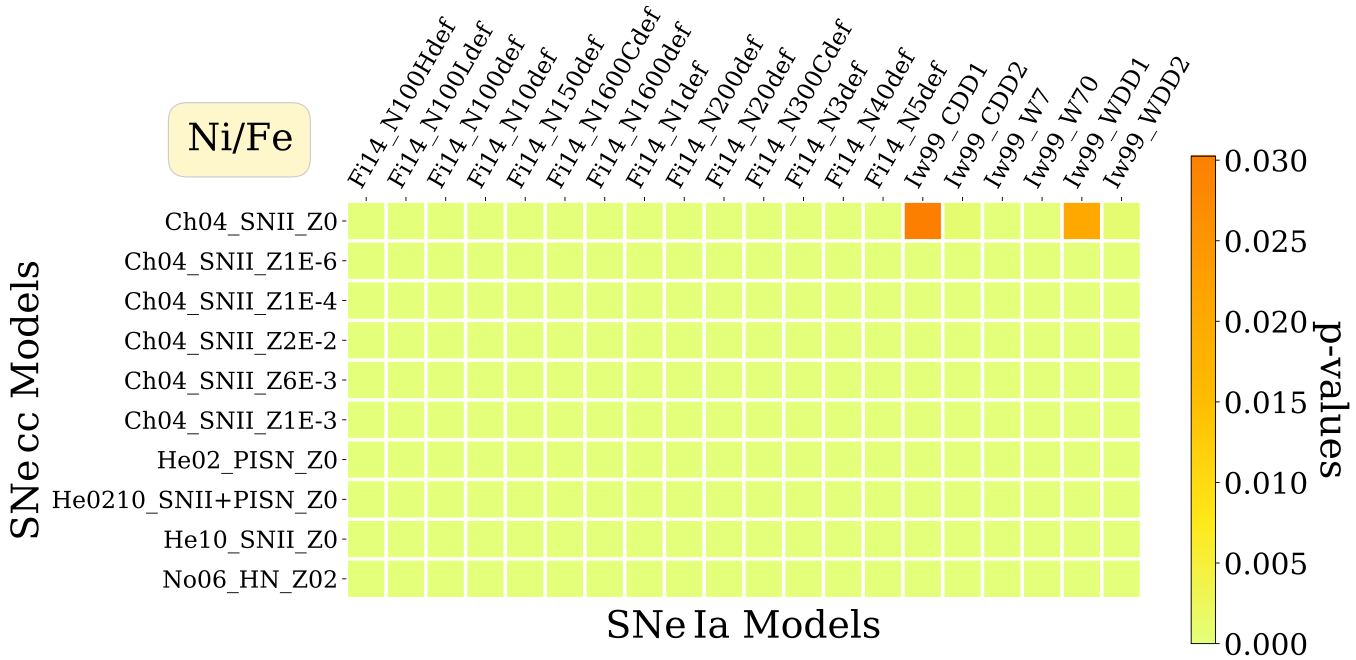

Figure 5. Same as Figure 1 but for Ni/Fe ratio.

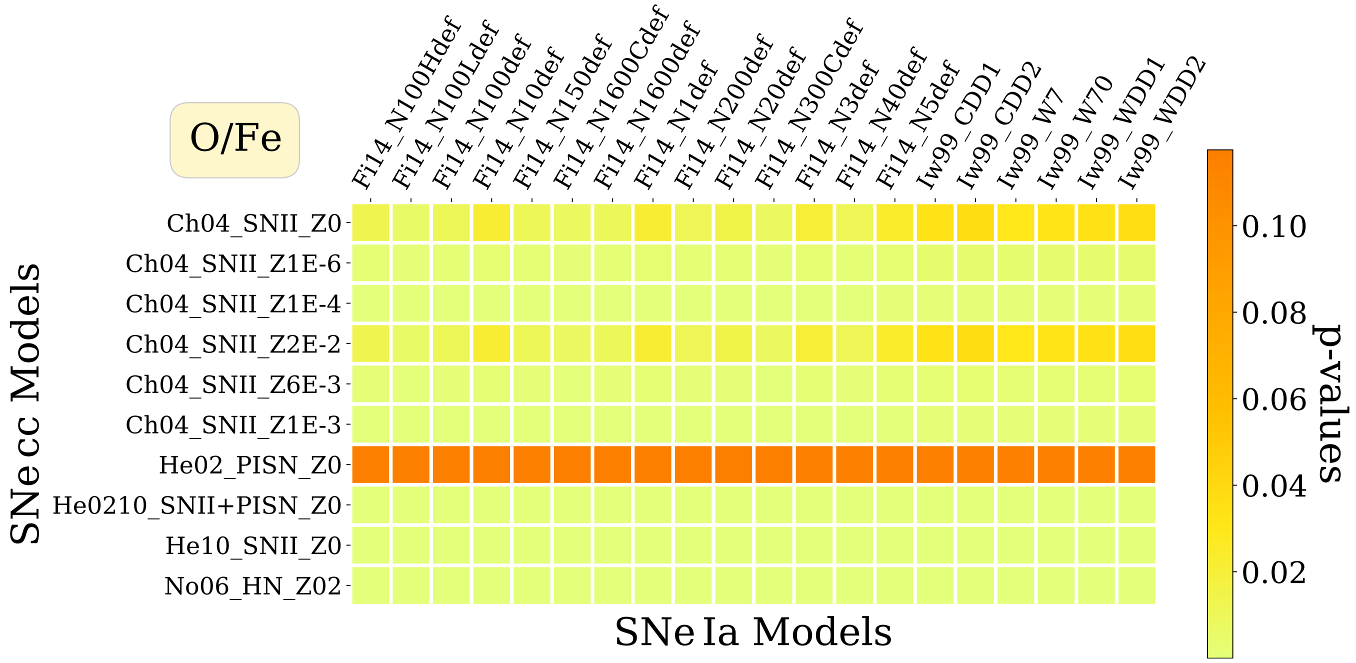

Figure 6. Same as Figure 1 but for O/Fe ratio.

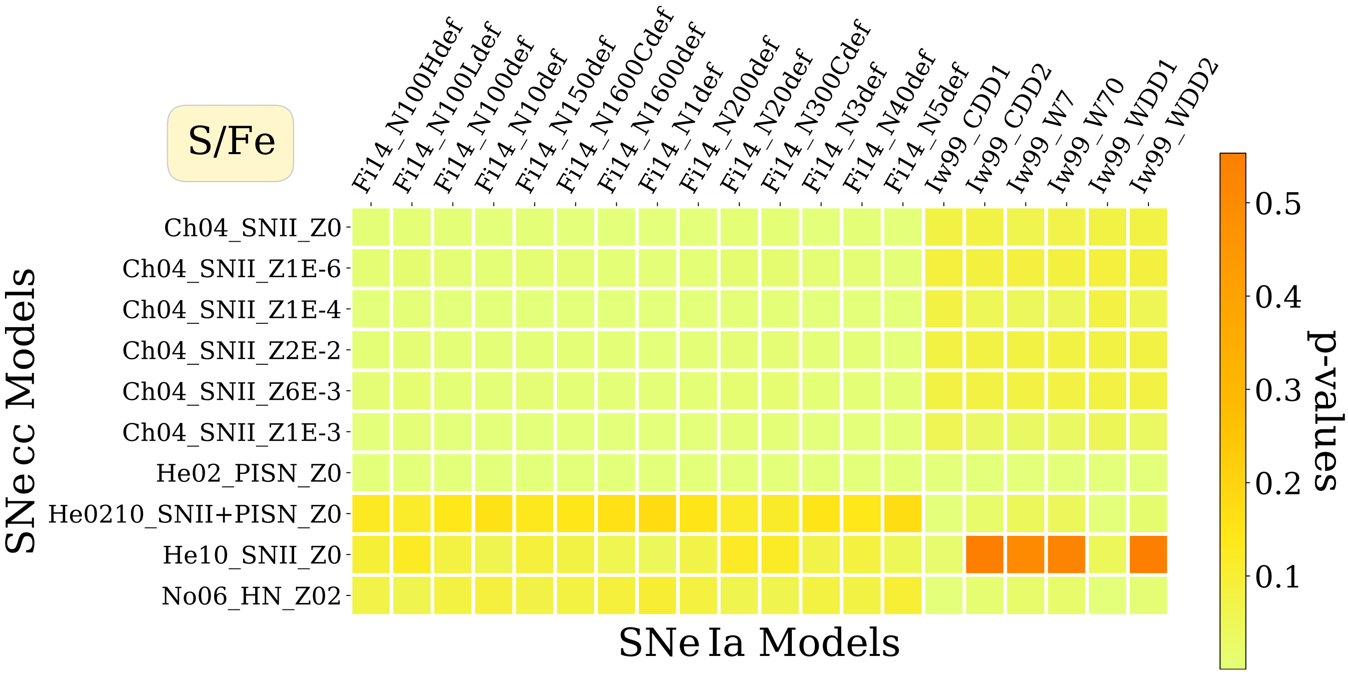

Figure 7. Same as Figure 1 but for S/Fe ratio.

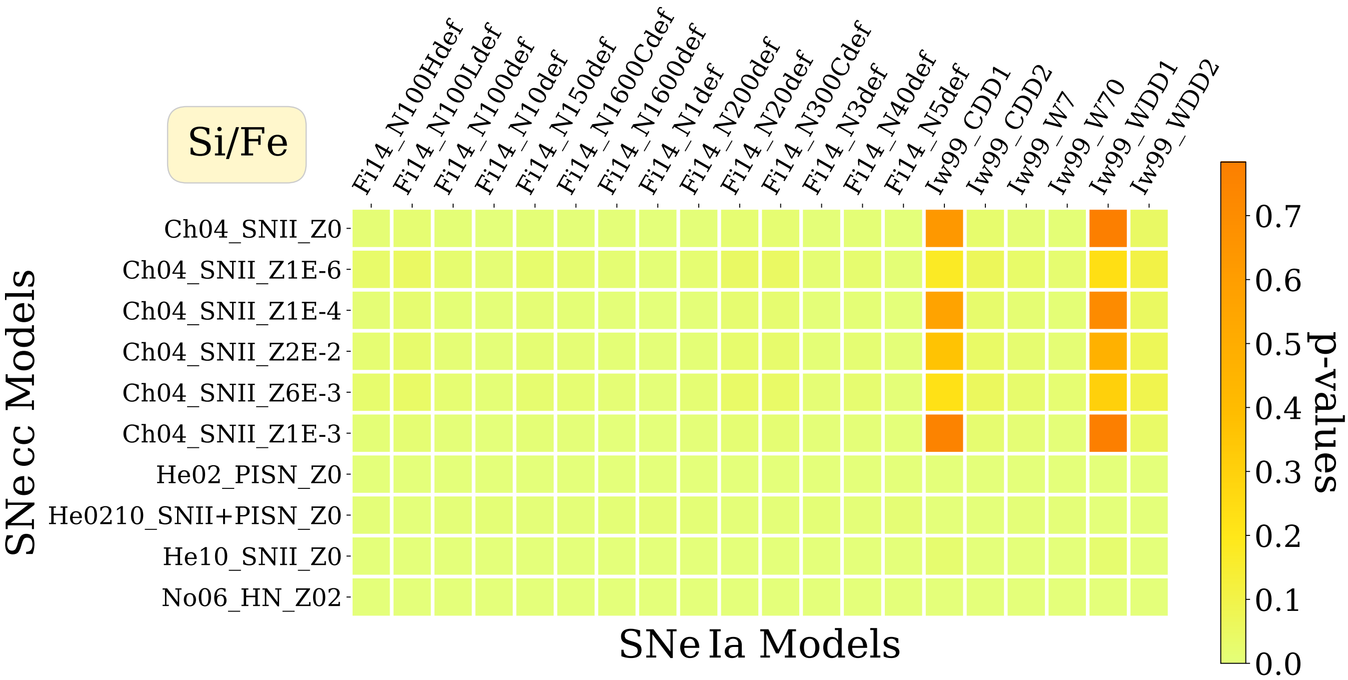

Figure 8. Same as Figure 1 but for Si/Fe ratio.

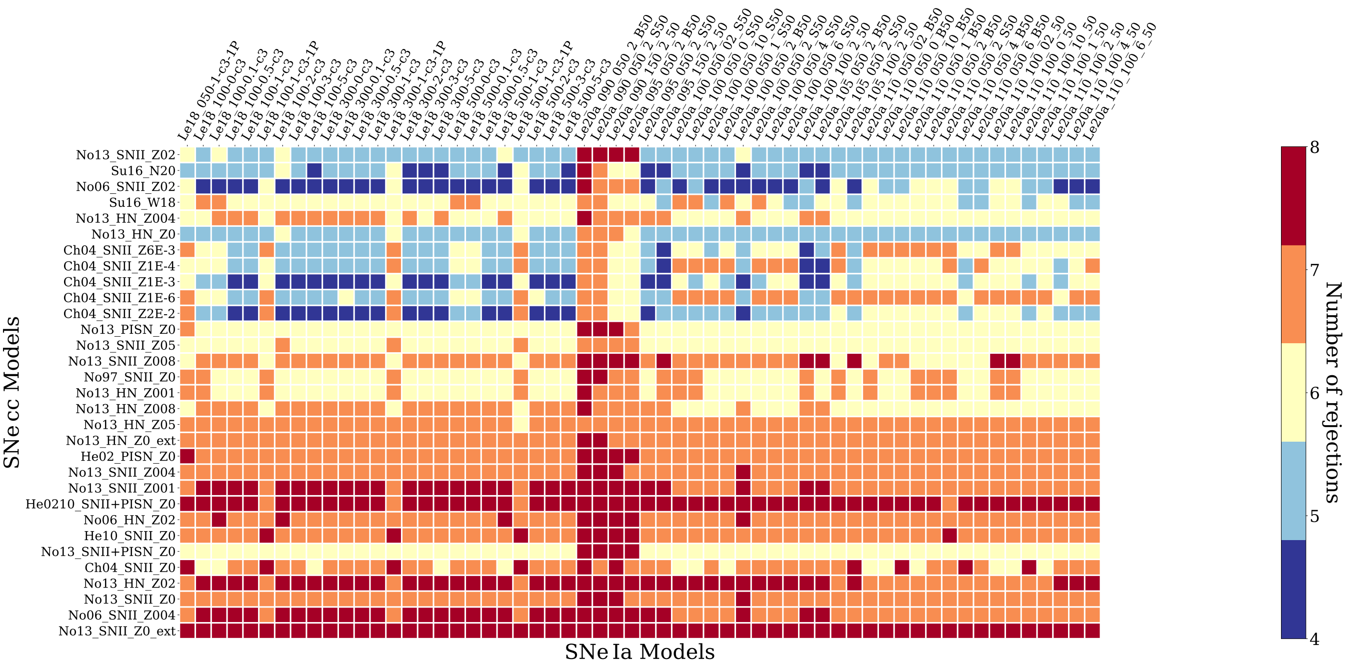

Figure 9. Number of times a model pair of SNIa+SNcc has been rejected at 2σ level confidence.

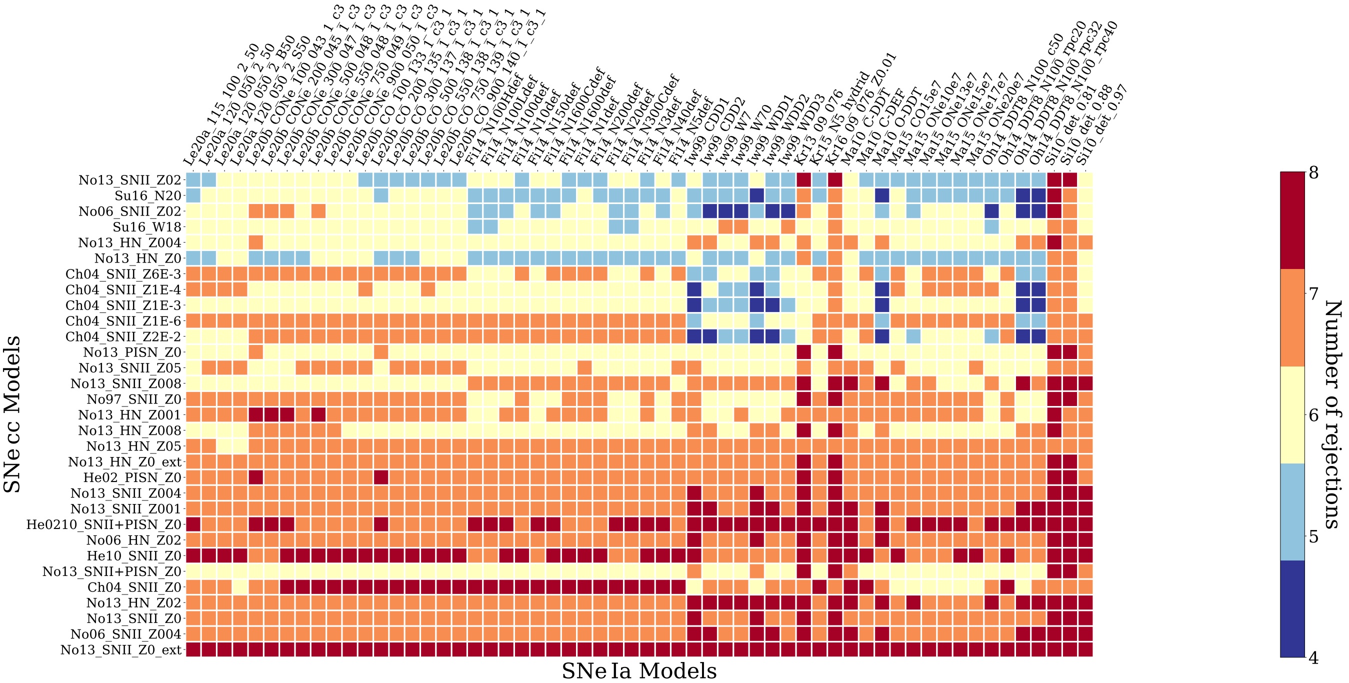

Figure 10. Number of times a model pair of SNIa+SNcc has been rejected at 2σ level confidence.

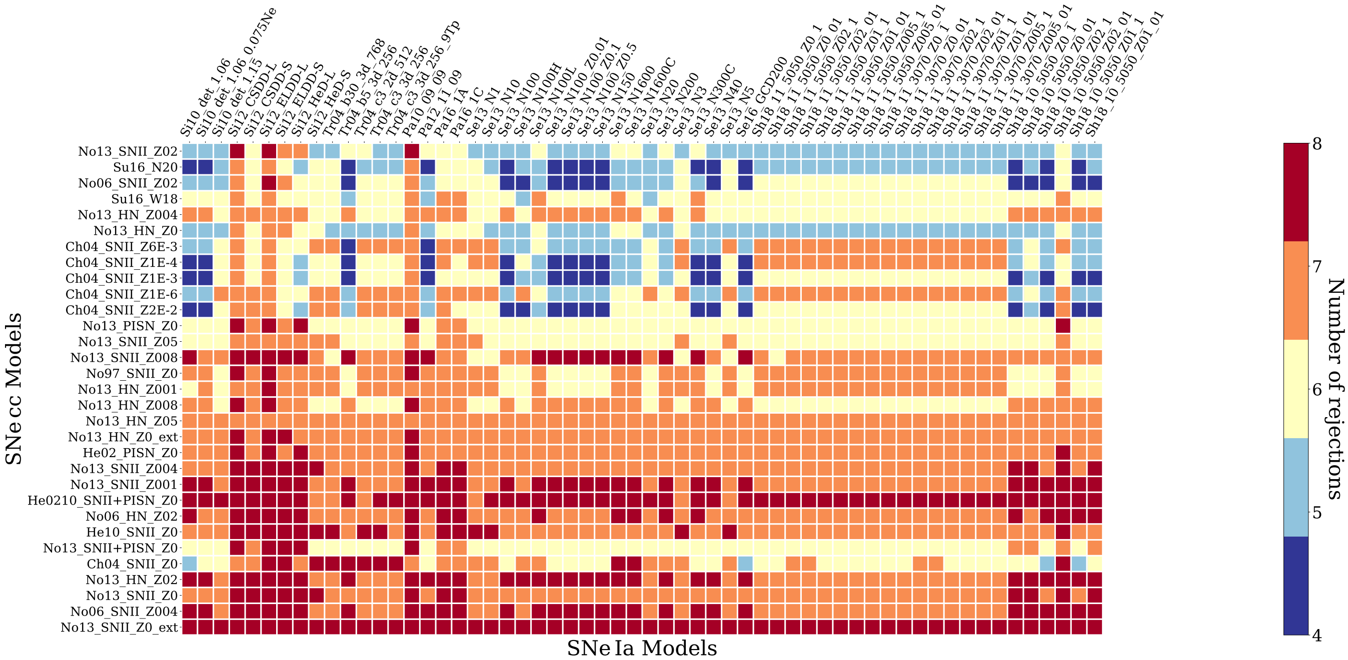

Figure 11. Number of times a model pair of SNIa+SNcc has been rejected at 2σ level confidence.

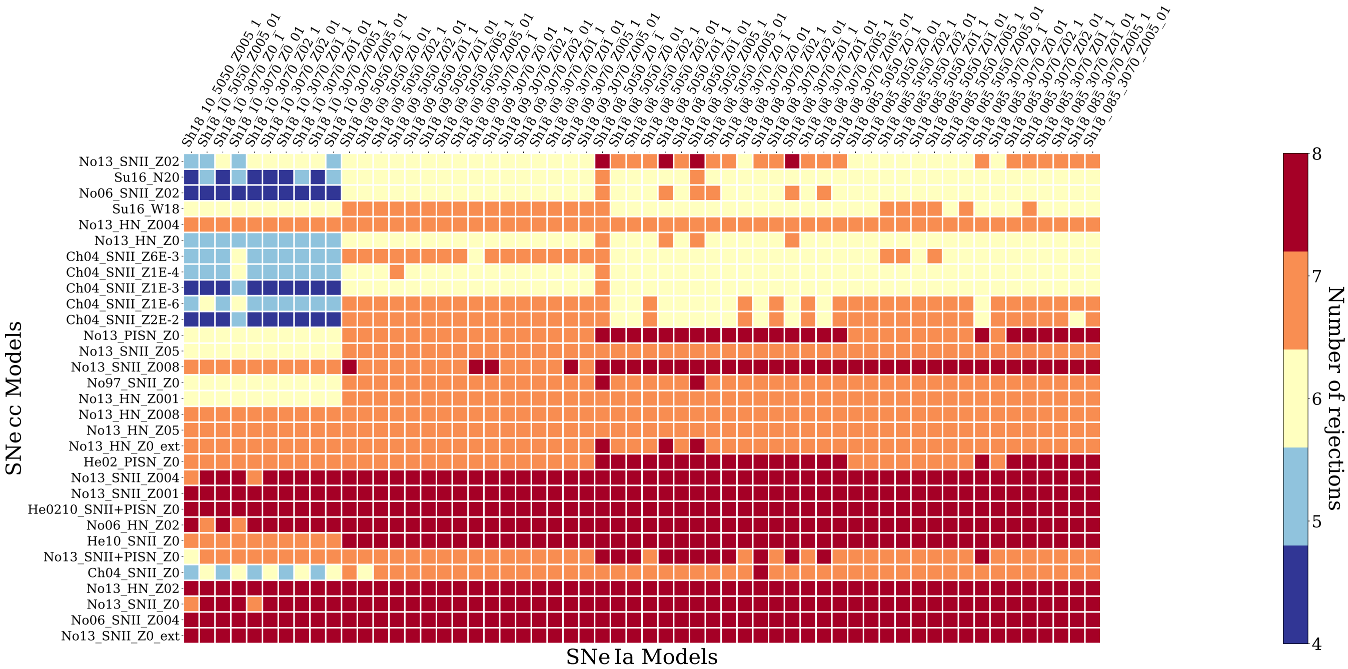

Figure 12. Number of times a model pair of SNIa+SNcc was rejected, using the p-value threshold of 0.05, which correspond to a 2σ level cutoff.